HHS Public Access

Author manuscript

Nat Genet. Author manuscript; available in PMC 2024 January 03.

Published in final edited form as:

Nat Genet. 2023 October ; 55(10): 1632–1639. doi:10.1038/s41588-023-01505-9.

Molecular Basis for Maternal Inheritance of Human Mitochondrial DNA

William Lee[1,†], **Angelica Zamudio-Ochoa**[1,†], **Gina Buchel**[1,†], **Petar Podlesniy**[2], **Nuria Marti Gutierrez**[3], **Margalida Puigròs**[2], **Anna Calderon**[2], **Hsin-Yao Tang**[4], **Li Li**[5], **Aleksei Mikhalchenko**[3], **Amy Koski**[3], **Ramon Trullas**[2], **Shoukhrat Mitalipov**[3], **Dmitry Temiakov**[1,*]

[1]Department of Biochemistry and Molecular Biology, Thomas Jefferson University; 1020 Locust St, Philadelphia 19107, USA

[2]Neurobiology Unit, Institut d'Investigacions Biomèdiques de Barcelona (IIBB-CSIC-IDIBAPS) and Centro de Investigación Biomédica en Red de Enfermedades Neurodegenerativas (CIBERNED); Barcelona, 08036, Spain

[3]Center for Embryonic Cell and Gene Therapy, Oregon Health & Science University; 3303 W Bond Avenue, Portland, Oregon 97239, USA

[4]Molecular & Cellular Oncogenesis Program, The Wistar Institute, Philadelphia, 3601 Spruce Street, Philadelphia, PA 19104, USA

[5]Department of Pathology, Thomas Jefferson University; 1020 Locust St, Philadelphia 19107, USA

Abstract

Uniparental inheritance of mitochondrial DNA (mtDNA) is an evolutionary trait found in nearly all eukaryotes. In many species, including humans, the sperm mitochondria are introduced to the oocyte during fertilization[1,2]. The mechanisms hypothesized to prevent paternal mtDNA transmission include ubiquitination of the sperm mitochondria and mitophagy[3,4]. However, the causative mechanisms of paternal mtDNA elimination have not been defined[5,6]. We found that mitochondria in human spermatozoa are devoid of intact mtDNA and lack mitochondrial transcription factor A (TFAM), the major nucleoid protein required to protect, maintain, and transcribe mtDNA. During spermatogenesis, sperm cells express an isoform of TFAM,

[*]Corresponding author. dmitry.temiakov@jefferson.edu.

Contributions:
Tissue collection: NMG, LL
Cloning: GB, WL, AZO
Droplet digital PCR: PP, MP, AC, RT
Protein purification: AZO
Cell culture, transduction, IH, CISH: WL
LC-MS/MS analysis: HYT, WL
Whole Genome Sequencing and data analysis: AM
Regulatory Oversight: AK
Experimental design: WL, AZO, GB, RT, SM, DT,
Writing – original draft: DT
Writing – review & editing: DT, WL, AZO, RT, MA, SM

[†]These authors contributed equally to this work

Competing interests:
Authors declare that they have no competing interests.

which retains the mitochondrial pre-sequence, ordinarily removed upon mitochondrial import. Phosphorylation of this pre-sequence prevents mitochondrial import and directs TFAM to the spermatozoon nucleus. TFAM relocalization from the mitochondria of spermatogonia to the spermatozoa nucleus directly correlates with the elimination of mitochondrial DNA, thereby explaining maternal inheritance in this species.

Uniparental inheritance of mtDNA is one of evolution's few enduring pillars. Except for some fungi and mussels, most eukaryotes inherit their mtDNA from a single parent, most commonly a mother. The uniparental mtDNA inheritance pattern evolved repeatedly, and a multitude of mechanisms have developed to exclude the paternal (sperm) mitochondria from a zygote[7]. This suggests the existence of selection pressure, as retaining the uniparental inheritance appears to be positively beneficial. However, the benefits of uniparental inheritance for fitness are not immediately clear. Intuitively, having genetically divergent copies of mtDNA may complicate their cooperation with the nuclear genome and generate "selfish" mtDNA molecules, which replicate efficiently but cannot support adequate energy production[8,9]. Indeed, heteroplasmy, or the presence of different mtDNA haplotypes, results in genetic instability and adverse physiological effects, behavioral and cognitive complications in mice[10].

Despite the overwhelming dominance of uniparental inheritance, the underlying molecular mechanisms that prevent biparental inheritance are not understood. Profound downregulation of mtDNA levels during spermatogenesis occurs in some non-human species[11,12], reaching zero in one report in mice[5]. It has also been reported that ubiquitination of the sperm mitochondria leads to their targeted degradation by the proteasome-dependent proteolytic machinery after fertilization in mammals[3]. Selective degradation of the paternal mitochondria by autophagy (a process known as mitophagy) in the embryonic cytoplasm has been documented in nematodes[4]. However, experiments show a lack of mitophagy in mammalian oocytes[5,6], and thus the mechanisms of maternal inheritance of human mtDNA remain obscure.

Previous studies reported a large variation of mtDNA copy number in human spermatozoa - from 1 to 1000 genomes per cell[13–15]. To accurately measure the mtDNA copy number in human sperm cells, we used Droplet Digital PCR (ddPCR), which allows a determination of the absolute number of DNA molecules in a cell (Fig. 1A). Because the method does not require isolation of the genomic material, and allows quantification of nuclear and mitochondrial genomes in the same sample with high analytical sensitivity and a limit of detection below a single genome copy per microliter of a sample, ddPCR is ideally suited for measuring low copy number nucleic acids[16]. Amplification targeted two single-copy genes in the nuclear genome (*TBP* and *TEFM*) and two mitochondrial genes – *CYTB* and *ND1* (Fig. 1B, C). We found that the sperm cells contain, on average, 0.58 copies of mtDNA (Fig. 1D). Analysis of the Whole Genome Sequencing (WGS) data of bulk DNA suggests that each spermatozoon contains, on average, 0.14 copies of mtDNA (Extended Data Fig. 1A, B and Extended Data Table 1), consistent with the ddPCR measurements. The copy number measurements have not been affected by mtDNA deletions, as verified by deep sequencing of long-range PCR products of bulk spermatozoa DNA and ddPCR experiments

using multiple primers annealing to the conserved regions of the mitochondrial genome (Extended Data Fig. 1C–F, Extended Data Table 2). Each spermatozoon contains 50–70 mitochondria, corresponding to less than 0.01 mtDNA molecules per mitochondrion. While extremely low, this number likely accounts for the background mtDNA detected in a few contaminating cells (namely leucocytes), which can harbor up to 100 mtDNA per cell in their mitochondria.

Using an orthogonal strategy, we performed *in situ* hybridization of mtDNA in human testicular tissue using RNAScope (Fig. 1E). This method allows the detection of single DNA molecules per cell. An intense signal corresponding to mtDNA was detected in the mitochondria of spermatogonia, undifferentiated germ cells at the periphery of the seminiferous tubules (Fig. 1E). The primary spermatocytes, the cells developed from spermatogonium during the second stage of spermatocytogenesis, showed coarse staining of mtDNA, indicating its reduction during sperm maturation. Finally, mature spermatozoa had no detectible mtDNA signal in the midpiece region, in agreement with our ddPCR analysis (Fig. 1E). We conclude that the mature human spermatozoa are essentially devoid of mtDNA, consistent with maternal inheritance of the mitochondrial genome in mammals[17].

We next looked at the presence of key proteins involved in transcription and replication of mtDNA in the mitochondria of human spermatozoa. We found that amounts of human mitochondrial RNA polymerase (POLRMT, or mtRNAP), the catalytic subunit of DNA polymerase Polγ, and transcription elongation factor, TEFM, were below the detection limit of Western blotting (Extended Data Fig. 2A). More importantly, these proteins were absent from all published complete spermatozoa proteomes[18–20]. These findings demonstrate that the spermatozoa mitochondria cannot maintain, replicate mtDNA, or synthesize RNA *de novo*. Unexpectedly, we found that human and monkey spermatozoa contain large amounts of the major mitochondrial nucleoid protein, transcription factor TFAM (Fig. 2).

Western blot assays revealed a particular form of TFAM, which was ~ 5 kDa larger than the mature (mitochondrial) TFAM from HEK293 cells (Fig. 2A). A previous study detected alternative splicing of TFAM mRNA during the spermatogonia maturation[21]. Indeed, we found that the mature sperm cells contain an alternatively spliced TFAM mRNA, not found in somatic cells (Fig. 2B). We mapped the 3’ UTR of this transcript and found that it is shorter than the isoform found in somatic cells and contains an abbreviated, ~ 8 nt long poly A-tail (Fig. 2C, Extended Data Fig. 2). In agreement with the previous data obtained for testis tissue[21], as the result of an alternative splicing event, the sperm TFAM mRNA features an additional exon (hereafter I^T) (Fig. 2B). However, the I^T exon does not alter the protein open reading frame, and thus the translation of the sperm mRNA isoform results in the synthesis of a full-size TFAM precursor (residues 1–246), as confirmed by LC-MS/MS analysis (Fig. 2D, Extended Data Fig. 3). Both human and Rhesus monkey sperm TFAM contain the peptides found in the mitochondrial targeting sequence (MTS, residues 1–42) but lack a partial tryptic fragment (evidence of protein maturation), suggesting that unlike the mitochondrial TFAM in somatic cells, this protein isoform does not undergo mitochondrial processing, during which this targeting sequence would be removed (Fig. 2D). These findings are consistent with analysis of the RNAseq database, which reveals the presence of the sperm-specific Exon I^T in mRNA exclusively from the testicular tissue (Extended Data

Fig. 4A). Likewise, human tissues proteomics data indicate the presence of the pre-sequence peptides only in spermatozoa and not in somatic tissues (Extended Data Fig. 4B).

TFAM localizes exclusively to the mitochondrial reticulum in somatic cells (Fig. 3A). In contrast, confocal microscopy reveals TFAM in the head of spermatozoa but not in the mitochondria at the midpiece region (Fig. 3B). This is consistent with the presence of an unprocessed mitochondrial targeting sequence in the sperm TFAM isoform, as established by LC-MS/MS analysis. Since TFAM is absolutely required for mtDNA maintenance, replication, and transcription, and the reduction of its expression is linked to mtDNA elimination in all animal models tested[22–27], the lack of TFAM in the spermatozoa mitochondria explains why these cells do not possess mtDNA.

Confocal microscopy revealed a nuclear localization of TFAM in the anterior half of the spermatozoa head, in proximity to a sperm-specific organelle, acrosome (Fig. 3B). However, a detailed analysis of TFAM localization using 3D reconstruction of the deconvolved images suggests a clear co-localization of TFAM with the spermatozoon nucleus and not with the acrosome (Fig. 3C). Further, immunogold labeling of TFAM revealed the presence of gold-stained TFAM in the nucleus of the sperm cells (Fig. 3D), but not in the sperm mitochondria, as evident from the analysis of the images taken (n=30) (Extended Data Fig. 5A, B).

Our data suggest that during sperm cell development, TFAM should switch its localization from mitochondria to the nucleus. We stained human testicular tissue with an anti-TFAM antibody (Fig. 3E–G). An intense TFAM signal was detected in the mitochondria of spermatogonia (Fig. 3G). In contrast, primary spermatocytes showed only traces of TFAM, which partially overlaps with TOM20, one of the translocases of the outer mitochondrial membrane, indicative of mitochondrial localization (Fig. 3F, G and Extended Data Fig. 5C). Closer to the lumen, the immature sperm cells - round spermatids – reveal intense DAPI staining of their compacted nuclei, which co-localized with the TFAM signal (Fig. 3F, G). We speculate that sperm TFAM may already be present in the nuclei of the primary spermatocytes but becomes visible only when “concentrated” by the nuclear condensation in spermatids. Remarkably, the re-location of TFAM from the mitochondria of immature sperm cells to the spermatozoa nucleus coincides with the disappearance of mtDNA observed during spermatogenesis (Fig. 1E).

Cytosolic translation of some yeast mitochondrial proteins is mediated by PUF proteins that recognize the 3’ UTRs sequences and direct the mRNAs to the ribosomes associated with the mitochondrial outer membrane to enable a co-translational import[28]. Assuming that a similar targeting system might function in other eukaryotes and considering that an alternatively spliced variant of TFAM mRNA has been found in sperm cells, we set out to investigate how the presence of the sperm-specific UTRs affects the trafficking of TFAM in spermatozoa. Transduction of HeLa cells with lentiviral constructs containing TFAM mRNA with either the sperm-specific (nuclear) or somatic (mitochondrial) 5’- and 3’- UTRs, or the mRNA lacking the UTRs altogether resulted in TFAM localization exclusively into the mitochondria, as evident by confocal microscopy (Fig. 4A, Extended Data Fig. 5D, E). In contrast, when the mitochondrial pre-sequence was deleted, TFAM localized to the cell

nucleus (Fig. 4B). We speculate that the nuclear localization of TFAM lacking mitochondrial pre-sequence results from a predicted nearly-consensus bipartite nuclear localization signal in TFAM[29].

When investigating TFAM trafficking in sperm cells, we observed an efficient accumulation of TFAM-mScarlet in the cytoplasm, visible by a progression of the red fluorescent signal from the sperm head to its tail (Fig. 4C). Interestingly, we did not detect TFAM accumulation in the nucleus or mitochondria (Fig. 4D). TFAM was localized in the cytoplasm of the sperm cells irrespective of the presence or absence of UTRs (Extended Data Fig. 6A). The extremely high packing density of the genomic material, about 10-fold higher than in somatic cells[30], could explain the absence of exogenous TFAM in the sperm nucleus. Indeed, overexpression of the sperm nuclear protein, histone H2B, shows cytoplasmic localization of this protein in sperm cells but nuclear localization in somatic cells (Extended Data Fig. 6 B, C). Notwithstanding, the import of proteins into sperm mitochondria appears active, as we detected mitochondrial localization of the overexpressed matrix protein TEFM and membrane protein TOM20 in the transduced spermatozoa (Extended Data Fig. 6 D, E). Most importantly, the lack of TFAM-mScarlet fluorescence signal in mitochondria of the transduced sperm cells suggests that the mitochondrial import of the overexpressed protein is being actively prevented.

To understand the reason behind the lack of TFAM import into the spermatozoa mitochondria, we transduced these cells with lentivirus carrying red fluorescent protein mScarlet fused to the mitochondrial pre-sequence of TFAM or of mtRNAP (Fig. 5A, B and Extended Data Fig. 7). While we observed mScarlet localization in sperm mitochondria when mtRNAP pre-sequence was used (Extended Data Fig. 7A), we detected no fluorescence signal inside mitochondria in the case of the TFAM pre-sequence (Fig. 5A), hinting at the key role of this region in sperm TFAM localization. Indeed, when Δ42-TFAM-mScarlet fusion with the mtRNAP pre-sequence was used, this protein was localized to spermatozoa mitochondria (Fig. 5B).

Discovering the crucial role of the pre-sequence in preventing the mitochondrial import of TFAM prompted us to search for posttranslational modifications in this region. LC-MS/MS analysis of human sperm TFAM identified phosphorylation of the residue S34 in the pre-sequence (Fig. 5C). Analysis of the human sperm phosphoproteome confirmed the presence of phosphorylation at S34 and, in addition, at S31 in the sperm TFAM pre-sequence[31]. Mitochondrial pre-sequence recognition is sequence-independent and based on its secondary structure (commonly an a helix) and the positive charge of this region[32]. Phosphorylation of S31 and S34 conserved in mammalian TFAM (Fig. 5D) is expected to bring a large negative net charge to the pre-sequence region and prevent mitochondrial import.

While the function of MTS phosphorylation is largely unknown, several reports indicate inhibition of protein translocation into mitochondria[33–35]. To confirm that the phosphorylation of the TFAM pre-sequence region plays a role in preventing mitochondrial import of TFAM in the sperm cells, we used a phosphomimicking TFAM variant in which the S31 and S34 residues were substituted to double aspartate residues ($TFAM^{S31DD/S34DD}$) to emulate the charge of the dianionic phosphate monoester of a phosphoserine residue

(Extended Data Fig. 8). In the control experiment, HEK293 cells transduced with the TFAM-mScarlet variant having serine to double alanine substitutions ($TFAM^{S31AA/S34AA}$) showed definitive mitochondrial localization of the protein (Extended Data Fig. 8A). In contrast, $TFAM^{S31DD/S34DD}$ was found predominantly in the nucleus of the transduced cells, an outcome observed for TFAM variant with the pre-sequence deletion (Fig. 4B), suggesting that its import to mitochondria was affected by the introduced phosphomimicking mutations (Extended Data Fig. 8B). To directly probe the effect of phosphorylation on localization of TFAM in spermatozoa, we substituted S31 and S34 residues with alanines (which are not targeted for phosphorylation) and transduced sperm cells with lentivirus carrying this TFAM variant. Using confocal microscopy, we found that $TFAM^{S31A/S34A}$ was localized exclusively to the sperm mitochondria (Fig. 5E). These data suggest that phosphorylation of the TFAM pre-sequence is necessary and required to prevent its import into the sperm mitochondria.

Maternal inheritance of mtDNA is a major paradigm that guides the existence and evolution of the vast majority of species; however, the molecular basis of this phenomenon and its benefits has remained unclear. Previous studies of human mitochondrial inheritance focused on post-fertilization mechanisms of elimination of paternal organelles and mtDNA from oocytes[3,36], while pre-fertilization mechanisms have never been reported. Here we demonstrate that phosphorylation-dependent re-localization of TFAM from the mitochondria to the nucleus of sperm cells during spermatogenesis results in mtDNA elimination and explains its maternal inheritance (Fig. 6). In the absence of mtDNA and active transcription, the presence and functional activity of OXPHOS complexes in mature spermatozoa could rely on increased stability of mitochondrial transcripts during spermatogenesis or a prolonged life of proteins composing the respiratory chain[37,38]. Indeed, several reports suggest a critical role of mitochondrial ATP synthesis in spermatozoa motility[39,40].

The discovery of TFAM re-localization has important implications for the fields of human fertility and germ cell therapy[41]. Spermatozoa that are deficient in nuclear TFAM could account for some cases of unexplained male infertility. Indeed, elevated mtDNA levels were found in the sperm of men with severe oligoasthenospermia[15]. Our findings suggest that the sperm isoform of TFAM can serve as a novel biomarker of male infertility and may have clinical implications.

Methods

Cell culture

HEK293, HEK293T, and HeLa cells were cultured in DMEM containing 10% (v/v) FBS and 1% (v/v) Penicillin/Streptomycin (all from Gibco) at 37 °C and 5% CO_2 in a humidified atmosphere. Adherent cells were harvested by incubation with 0.25% trypsin-EDTA. Cells were passaged and maintained at a 2.5×10^5 cells/ml density.

Gamete collection and analysis.

Human subjects donations and study protocols were approved by Oregon Health & Science University (OHSU) IRB. Prior to gamete donations, informed consent was obtained from

all human subjects on study-specific consent forms. Oversight defining research on human gametes and preimplantation embryos at OHSU undergoes rigorous regulatory review. All sample collections and sample preparations for analysis were performed at OHSU.

Semen collection was obtained via at-home semen collection kits or at OHSU Fertility Clinic. All participants have given informed, written consent. Participants were instructed to abstain from ejaculation for 24 h prior to collection. The ejaculate was maintained at body temperature until processing. Sperm samples were obtained from normozoospermic fertile adult donors (34–43 yo). The samples were liquefied for 30–60 min at room temperature (RT). After liquefaction, the semen was loaded on AllGrad 90% (Cooper Surgical, #AG90–100) gradient solution and centrifuged at 250 g for 15 min. The pellet containing spermatozoa was then rinsed in Quinn's sperm washing medium (Cooper Surgical, #ART-1006) and centrifuged again at 200 g for 6 min. The cells were counted using a hemocytometer and observed for the presence of the contaminating cells.

All animal experiments followed NIH Guidelines for Animal Research and approved by OHSU Institutional Animal Care and Use Committee. Sperm from the adult Rhesus macaque (*Macaca mulatta*) was collected as described previously [42].

Measurement of the absolute copy number of mtDNA

Purified human sperm cells (4,000,000 cells in 2 μl) were mixed with 8 μl of the pre-warmed lysis solution containing 10 M Urea and 30 mM DTT and incubated for 5 min at 95°C. Upon incubation, the lysed cells (5 μl) were transferred into a 1.5 ml tube containing 1 ml of DNA/RNA/protein solubilization reagent 100ST (DireCtQuant), mixed by vortexing, and incubated for 10 min at 95°C to complete the lysis and to dilute the sample to the optimal concentration of Urea (less than 50 mM). The resulting sample containing 2,000 lysed spermatozoa cells per μl of solution was used to measure the absolute copy number of mtDNA by Droplet Digital PCR (ddPCR). MtDNA was amplified using two primer pairs, mt64-ND1, and mt92-CYTB (Extended Data Table 3), which target two opposite regions of the mtDNA genome, as described[43].

The droplet reaction consisted of 1x QX200™ ddPCR™ EvaGreen Supermix (1864033, Bio-Rad), a 0.1 μl aliquot of the target sample, and TBP73 (95 nM) and TEFM88 (140 nM) primers for genome analysis, or mt64-ND1(100 nM) and mt92-CYTB (135 nM) primers for mtDNA analyses. A restriction enzyme digestion was performed prior to partitioning into droplets by adding the Fast Digest enzymes HaeIII and MseI (0.5 U each) into the ddPCR reaction for nuclear genome and AluI (1 U) for mtDNA amplification. The reactions were incubated for 15 min at 37° C. Non-template controls were included in each analysis plate to monitor possible reaction contamination. The PCR amplification was performed using the C1000 Touch Thermal Cycler (Bio-Rad) and the following thermal profile: 95° C 5 min; (95° C 30 sec; 60° C 1 min) 40 repeats; 4° C 5 min; 90° C 10 min.

To test if mtDNA quantification is influenced by the presence of mtDNA molecules with deletions, the mtDNA copy number in sample #4 was quantified with eight primer pairs targeting regions inside or outside the common mtDNA deletions following the same ddPCR protocol described above.

The data analysis was performed with QuantaSoft Analysis Pro v1.0 using thresholds to distinguish single and double-positive droplet populations. The number of genomes was calculated by averaging the DNA copy number obtained using TBP73 and TEFM88. To determine the mtDNA amount per haploid genome in a sperm cell, the number of mtDNA copies obtained with the mt64-ND1 or the mt92-CYTB amplicon was divided by the number of genomes measured in the same sperm sample. Simple or multiplex analyses were performed using the QX200 Digital Droplet PCR platform (Bio-Rad Laboratories).

DNA extraction from bulk samples

DNA was extracted from 15–30 million spermatozoa and white blood cells using a Gentra Puregene DNA purification kit (Qiagen, 158023) according to the manufacturer's instructions. To facilitate DNA extraction from spermatozoa, 150 mM dithiothreitol was added to the cell lysis solution during overnight incubation at 55° C with proteinase K.

Whole Genome Sequencing and mtDNA copy number analysis

To analyze mtDNA copy number in bulk sperm and blood samples, freshly extracted DNA was normalized to 1 μg in 25 μl of Resuspension buffer (Illumina)and used for the library preparation with Illumina DNA PCR-free kit following manufacturer's instructions. Paired-end sequencing was performed as 2×150 bp at an average autosome coverage depth of 4.2X on the Illumina NextSeq 1000. Genome Analysis Toolkit (GATK) preprocessing steps were applied to raw sequencing reads to produce BAM ready for further analysis. These included the generation of uBAM via FastqToSam (Picard tools, v2.26.9; http://broadinstitute.github.io/picard), marking adapters via MarkIlluminaAdapters, converting uBAM to fastq via SamToFastq, mapping to GRCh38 genome assembly using BWA-MEM (v0.7.17, https://arxiv.org/abs/1303.3997) and merging BAM and uBAM with MergeBamAlignment. Aligned reads were coordinate-sorted with SortSamSpark (GATK v4.2.6.1), and the duplicate reads were marked with MarkDuplicatesSpark (GATK v4.2.6.1)[44]. The resulting BAMs were filtered to retain alignments with mapping quality >30 to remove genomic reads that could be mapped to both mtDNA and NUMTs and were analyzed for autosome and mtDNA coverage breadth and depth with Samtools (v1.14)[45]. The resulting coverage data set was used for downstream analysis in R (v4.2.2, https://www.r-project.org/) and Integrated Genomics Viewer (v2.11.9)[46]. As there is only one copy of autosomal DNA in mature spermatozoa and are two copies in an average white blood cell, the mtDNA copy number was inferred as:

$$mtDNA\ copy\ number(sperm) = \frac{mean\ mtDNA\ coverage\ depth}{mean\ autosomal\ DNA\ coverage\ depth}$$

$$mtDNA\ copy\ number(blood) = \frac{mean\ mtDNA\ coverage\ depth}{mean\ autosomal\ DNA\ coverage\ depth} * 2$$

Long-range PCR and whole mtDNA sequencing

To test for the presence of a full-length mtDNA in bulk spermatozoa DNA, long-range PCR amplifying full mtDNA in one reaction was performed using TaKaRa LA Taq DNA

Polymerase (Takara Bio), and primers shown in Extended Data Table 3, as described previously[47]. PCR conditions were 94ºC 2 min; (98° C 20 sec; 68° C 20 min) 30 cycles; 72° C 10 min.

Amplified long-range PCR products were normalized to 0.2 ng/μl, and 1 ng was used for library preparation with the Nextera XT DNA kit (Illumina) following the manufacturer's protocol. Paired-end sequencing was performed as 2×150bp at an average coverage depth of 12,167X on the Illumina NextSeq 1000. Genome Analysis Toolkit (GATK) preprocessing steps were applied to raw sequencing reads to produce BAM ready for further analysis, as described above.

Chromogenic In Situ Hybridization Assay (CISH) using human testicular tissue

Human testicular tissues were from three patients with testicular cancer. The leftover tissue was routinely stored at the Department of Pathology at Thomas Jefferson University Hospital and then provided for this study, which does not require IRB review because it does not qualify as human subjects research as per 2018 Common Rule at 45 CFR 46.102(e)(1). The patients were 28–29 yo and had no history of mitochondrial disease. Non-neoplastic human testicular parenchyma from the orchiectomy specimens was obtained. The tissues were sectioned at 4 μm in thickness, away from the tumor, and mounted onto slides. The tissues were fixed with 10% formalin for 24 h, immersed in a series of various concentrations of ethanol (70, 80, 95, 100%) and xylene, followed by embedding into paraffin blocks with paraffin wax. Hematoxylin and eosin (H&E) staining has been performed. The H&E slides of testicular tissue were reviewed by a pathologist. The sections with normal spermatogenesis were marked, and adequate unstained sections were obtained from the formalin-fixed paraffin-embedded (FFPE) blocks for CISH and IHC.

CISH with mtDNA in testicular tissues was performed exactly as described in the manufacturer's protocol (Advanced Cell Diagnostic), using RNAscope 2.5 HD Assay BROWN Detection Kit and Hs-MT-COX1-sense probe (#478051; ACD). The signal was developed by incubation with DAB (3,3′-diaminobenzidine) for 10 minutes at RT and counterstained with hematoxylin (Sigma), followed by a wash in 0.02% ammonia water before mounting. Digital Images were obtained using an Olympus BX60 microscope at 20X magnification and the cellSens imaging software (Olympus).

Mitochondria isolation

HeLa cells were gently homogenized with 25 strokes using a Teflon homogenizer (Thomas Scientific) in 7.5 ml of HES buffer (20 mM HEPES, pH7.2, 0.25 M sucrose, and 0.1 mM EDTA), supplemented with 1 mM DTT, 0.1 mg/ml BSA, and 0.1 mM PMSF. Homogenates were centrifuged at 2,000 g for 5 minutes at 4 °C. Supernatants were collected and centrifuged again at 10,000 g for 12 minutes. The crude mitochondria were resuspended in HES buffer and further purified by a sucrose step gradient separation (15/23/34/60% sucrose in 20 mM HEPES, pH 7.2, 0.1 mM EDTA) at 100,000 g at 4 °C for 1 h. The purified mitochondria were resuspended in 100 μl of HES buffer, aliquoted, and stored at −20 ºC.

RNA purification

To extract the RNA from human spermatozoa (~80 million cells in 100 μl), they were homogenized by vortexing with 100 mg of 0.2 mm stainless steel beads (Next Advance) in Lysis Buffer (Thermo Scientific), supplemented with guanidine thiocyanate and 2% 2-mercaptoethanol, for 5 minutes at RT. The RNA was isolated from the lysate using the GeneJET RNA Purification Kit (Thermo Scientific), aliquoted, and stored at −80° C. To extract the RNA from HEK293 cells, they were lysed in 1 ml of TRI Reagent (Invitrogen) for 5 minutes at RT. 1-Bromo-3-chloropropane (100 μl) was added, vortexed for 15 seconds, and incubated for 10 minutes at RT. The lysate was then centrifuged at 12,000 g for 15 minutes at 4° C to separate the RNA-containing aqueous phase. The RNA was precipitated by mixing the aqueous phase with isopropanol and centrifuged at 12,000 g for 15 minutes at 4° C. The RNA pellet was washed with 75% ethanol and air-dried before resuspending in DEPC-treated water. The purified RNA was aliquoted and stored at −80° C.

Mapping of the 3’ UTR region of the mitochondrial and sperm isoform of TFAM

RNA samples were first treated with dsDNAse (Thermo Fisher Scientific) to remove DNA contamination. The 3’ ends of the sperm and HEK293 TFAM mRNA species were mapped by 3’ RLM-RACE using the FirstChoice RLM-RACE Kit (Ambion) with modifications. The RNA adaptor provided by the kit was phosphorylated on its 5’ end using T4 Polynucleotide Kinase (NEB). RNA (1 μg) was ligated to the 5’-phosphorylated RNA adaptor using T4 RNA Ligase (Ambion). Following ligation, the TFAM mRNA was amplified by RT-PCR using the SuperScript IV One-Step RT-PCR System (Thermo Fisher Scientific). The RT-PCR reaction was further amplified by PCR using inner primers (Extended Data Table 3).

LC-MS/MS analysis

To reduce the complexity of the sample for LC-MS/MS analysis, the band representing sperm TFAM was excised from 10% PAGE. Spermatozoa cells (~ 5 million) were lysed in the SDS sample buffer by sonication. Recombinant human TFAM was used as a protein marker to excise the band representing the sperm TFAM isoform. The excised protein band was washed and subjected to trypsin digestion. The gel bands were treated with tris(2-carboxyethyl)phosphine, alkylated with iodoacetamide, and the protein was digested with trypsin. Tryptic digests were analyzed by LC-MS/MS using a Q Exactive Plus or Q Exactive HF mass spectrometer (ThermoFisher Scientific) coupled with a Nano-ACQUITY UPLC system (Waters) as previously described [48,49]. Peptides and proteins were identified using MaxQuant [50]. MS/MS spectra were searched against the UniProt human or rhesus macaque protein database and a common contaminant database using full tryptic specificity with up to two missed cleavages and static carbamidomethylation of Cys. Variable modifications included in the search were oxidation of Met, deamidation of Asn, and protein N-terminal acetylation. To identify the TFAM maturation site in HEK293 mitochondria, a semi-tryptic search was performed. To identify unknown PTMs, the data were analyzed using the open search function of pFind 3.1.5 [51] with a precursor and fragment mass tolerance of 10 ppm. Consensus identification lists were generated with false discovery rates set at 1% for protein, peptide, and site identifications.

Northern blotting

The sperm and HEK293 RNA samples were diluted in a loading buffer (95% formamide, 5 mM EDTA, 0.025% SDS, 0.025% bromophenol blue, and 0.025% xylene cyanol) and heated at 95°C for 3 minutes to further denature samples before loading. RNA (1 μg) was loaded onto a 6% PAGE containing 6M Urea in 1X Tris-Borate-EDTA (TBE) buffer. HEK293 RNA (50 ng) was loaded onto the gel, and detection of 18S rRNA was used as a size marker. The RNA species were transferred onto a Hybond-H+ membrane (GE Healthcare) in 1X TBE buffer and crosslinked by UV exposure for 2 minutes upon electrophoresis. The DNA probes (Extended Data Table 3) at 500 nM were 5'-[^{32}P]-labeled using T4 Polynucleotide Kinase (NEB) and hybridized to the membrane overnight at 37°C in PerfectHyb™ Plus Hybridization Buffer (Sigma-Aldrich). The membrane was washed twice with 2X SSC buffer (Sigma-Aldrich), dried, and visualized by autoradiography using PhosphorImager (GE Healthcare).

Western blotting

Spermatozoa (~ 5 million cells) were lysed in 100 μl of 1x Laemmli sample buffer containing 10% 2-Mercaptoethanol by sonication. Proteins were separated using 12 %SDS-PAGE and blotted onto a polyvinylidene difluoride membrane (GE Healthcare). The membrane was blocked in 5% milk/PBS for 1 h followed by overnight incubation with mouse monoclonal anti-TFAM antibody (Abcam, #ab119684, 1:1000 dilution) at 4 °C. PolG was detected using an anti-PolG antibody (Abcam, #128899, 1:1000). TEFM was detected using home-raised mouse monoclonal antibody against human TEFM (1:1000), while mtRNAP - using home-raised rabbit polyclonal antibodies against human Δ150 mtRNAP (1:1000). VDAC was detected using anti-VDAC antibody (Cell Signaling Technology, #4661, 1:1000). The membrane was washed three times with PBST (1X PBS and 0.1 % Tween) and incubated with IRDye 680RD-labeled goat anti-mouse antibody (LI-Cor, #926–68070, 1:10,000 dilution) or IRDye 800CW-labeled goat anti-Rabbit IgG Secondary Antibody (LI-Cor, #926–32211, 1:15000) for 1 h at RT. The membrane was washed 6 times with PBST and imaged using the Infrared Imaging System Odyssey FC (LI-Cor).

Cloning

For the lentiviral expression, the DNA region encoding TFAM-mScarlet fusion was excised from the pcDNA3-TFAM-mScarlet plasmid (Addgene ref #129573) using BamHI and EcoRI endonucleases and inserted into the pWPXL plasmid (Addgene ref #12257). To obtain the TFAM construct containing the 3'mitoUTR (3'mitoUTR_TFAM-mScarlet_pWPXL), human heart cDNA (Zyagen, HD-801) was PCR-amplified using primers shown in Extended Data Table 3, and the amplicon cloned into a pT7Blue cloning vector (Novagen). Restriction sites (EcoRI/NdeI) were added through amplification by PCR to insert the fragment into the TFAM-mScarlet/pWPXL plasmid. The 5'mitoUTR was cloned into the TFAM-mScarlet/pWPXL or the 3'mitoUTR_TFAM-mScarlet_pWPXL plasmid using megaprimers following (here and below) the QuikChange II XL Site-Directed Mutagenesis Kit (Agilent) protocol for large insertions. The Megaprimers for the 5' mitoUTR were synthesized by amplifying DNA extracted from HEK293 cells using primers (Extended Data Table 3). To obtain the TFAM constructs containing the

3’ and/or 5’ sperm TFAM UTRs, megaprimers were synthesized and cloned into the TFAM-mScarlet_pWPXL plasmid. The Megaprimers were synthesized by amplifying DNA extracted from HEK293 (Extended Data Table 3). Deletion of the TFAM MTS (residues 1–42, Δ42TFAM-mScarlet) was performed using the QuikChange II XL Site-Directed Mutagenesis kit in 3’5’mitoUTR_TFAM-mScarlet_pWPXL.

TOM20 and H2B Type 1A ORFs were amplified by PCR from human heart cDNA (Zyagen). The amplicons were cloned into the pT7Blue cloning vector (Novagen) using the megaprimers (Extended Data Table 4). The protocol for large insertions was followed to insert TOM20 or H2B in place of the TFAM gene TFAM-mScarlet_pWPXL plasmid. The MTS^{TFAM}mScarlet_pWPXL construct was generated by removing the TFAM sequence (residues 43–246) from the TFAM-mScarlet_pWPXL construct described above. To substitute the TFAM MTS with the mtRNAP MTS and generate the MTS^{pol}Δ42TFAM-mScarlet construct, we generated megaprimers by PCR amplification of the MTS region (residues 1–45) of mtRNAP. The megaprimers were inserted into the TFAM-Scarlet_pWPXL plasmid.

Human mtRNAP (residues 1–1230) was cloned into the pWPXL vector to obtain the mtRNAP_pWPXL construct. Megaprimers containing the mScarlet gene were used to obtain the MTS^{Pol}-mScarlet-mtRNAP-pWPXL construct. The MTS^{pol}mScarlet_pWPXL construct was obtained by excising the MTS^{Pol}-mScarlet region using PmeI and XcmI and ligating this fragment into the pWPXL plasmid. Substitutions of the serine residues in the TFAM MTS (S31A/S34A), (S31A,P32A/S34A,F35A, “$TFAM^{S31AA/S34AA}$”), and (S31D,P32D/S34D,F35D, “$TFAM^{S31DD/S34DD}$”),) were performed using QuikChange II XL Site-Directed mutagenesis kit in the TFAM-mScarlet_pWPXL construct.

Generation of lentiviral particles

In brief, 15 μg of the vector plasmid containing the gene of interest, 10 μg of the packaging construct plasmid psPAX2 (Adgene #12260), and 5 μg of VSV-G envelope expressing plasmid pMD2.G (Addgene #12259) were co-transfected into HEK293T cells using calcium phosphate transfection. The transfection mix was removed after 16 h and replaced with the complete media. The lentiviral particles were harvested after 24 and 48 h incubation, filtered through a 0.45 mm filter, and concentrated by ultracentrifugation before being stored at −80 °C. The infection efficiency of the viral particles was tested on HEK293T cells to ensure over 90% infection.

Lentiviral transduction of human somatic cells and spermatozoa

HeLa cells were seeded at 415 cells/mm^2 in a 6-well plate to reach 90% confluency over 24 h before transduction. Upon incubating the lentiviral particles with HeLa cells for 16 h, the cells were washed twice with PBS and resuspended in a fresh complete culture medium. Transduced HeLa cells were obtained after 48 h post-transduction and resuspended in a fresh culture medium to be seeded for immunofluorescence (IF) staining. Viruses generated using the pWPXL vector were used as control.

To transduce the sperm cells, lentiviral particles were added to 1 ml of spermatozoa (~10^7 cells) in a capacitation medium and incubated for 3–48 h. The transduced sperms were

centrifuged at 600 g for 5 min, and the sperm pellet was resuspended in PBS to be further spotted on coverslips for IF staining.

Immunofluorescence staining

Before staining, HeLa cells were seeded on poly-L-lysine (Gibco) coated glass coverslips overnight, while human spermatozoa were spotted and air-dried directly on the coverslips after isolation. The samples were fixed with 4% paraformaldehyde (Thermo Fisher Scientific) for 20 minutes at RT, washed with PBS, permeabilized in PSB solution containing 0.25% Triton X-100 (Sigma-Aldrich) for 5 minutes, and blocked with PBS solution containing 1% BSA (Sigma-Aldrich) and 0.1% Triton X-100 for 1 h at 37 °C. After washing with PBS, the samples were blocked with 1% BSA-PBS solution for 1 h at 37 °C. The prepared coverslips were incubated with the following primary antibodies prepared in mouse monoclonal anti-TFAM antibody (Abcam, #ab119684, 1:500) or monoclonal anti-TOM20 antibody (Cell Signaling Technology, #42406S, 1:500) in 0.1% Triton X-100 overnight at 4 °C. The coverslips were washed three times with 0.1% Triton X-100 at 4 °C for 5 min, and the secondary antibody, donkey anti-mouse Alexa Fluor 555 (Abcam #ab150110, 1:2000) or goat anti-rabbit Oregon Green 488 (Invitrogen #O-11038, 1:2000) was added for 2 h at RT. The coverslips were then counterstained with 300 nM DAPI (Invitrogen) and mounted with Prolong Glass antifade (Invitrogen). Digital images were obtained using a Nikon A1R+ confocal microscope at 60x magnification. The images were analyzed using the Fiji processing package on ImageJ.

Transmission Electron Microscopy

Purified human spermatozoa were collected and fixed with a freshly made fixative containing 3% paraformaldehyde and 0.1% glutaraldehyde in 0.1M phosphate buffer with 4% sucrose (pH 7.2). After washing with 0.1M phosphate buffer with 4% sucrose, 0.1M glycine was added to quench the unbonded aldehyde group. The cells were dehydrated in graded series of ethanol on ice and embedded in LR White (Electron Microscopy Sciences, Hatfield, PA). The samples were polymerized under UV light (360nm) at −10°C for 48 h, followed by 12 h at RT. The 90 nm-thin sections were cut and mounted on Formvar-Carbon coated 200 mesh nickel grids. The grid was incubated with an anti-TFAM antibody (1:1000, Abcam, #ab119684) in PBS with 1% BSA, and 0.05% Tween 20, for 2 h at RT, then overnight at 4°C. Upon washing, the anti-mouse secondary antibody conjugated with 18 nm gold (1:15, Colloidal Gold AffiniPure Goat Anti-Mouse IgG (H+L, EM Grade, Jackson ImmunoReasearch Laboratories, Inc.,) were added in PBS with 1% BSA, and 0.05% Tween 20, and incubated for 1h. After washing, the grids were stained with uranyl acetate and lead citrate by standard methods, imaged with Talos120C transmission electron microscope (Thermo Fisher Scientific), and recorded using Gatan (4k x 4k) OneView Camera with software Digital Micrograph (Gatan Inc).

Statistics and Reproducibility

All experiments have been repeated at least three times. Experiments presented in figs 1e, 2a–b, 3a–b, 3f–g, 4a–d, 5a–b, 5e; Extended Data figures: 2a, 5d–e, 6a–e, 7a–d, 8a–b were repeated at least three times. Over 60 images were taken in the experiment shown in fig. 3d and Extended Data figures 5a,b. The representative images are shown.

Extended Data

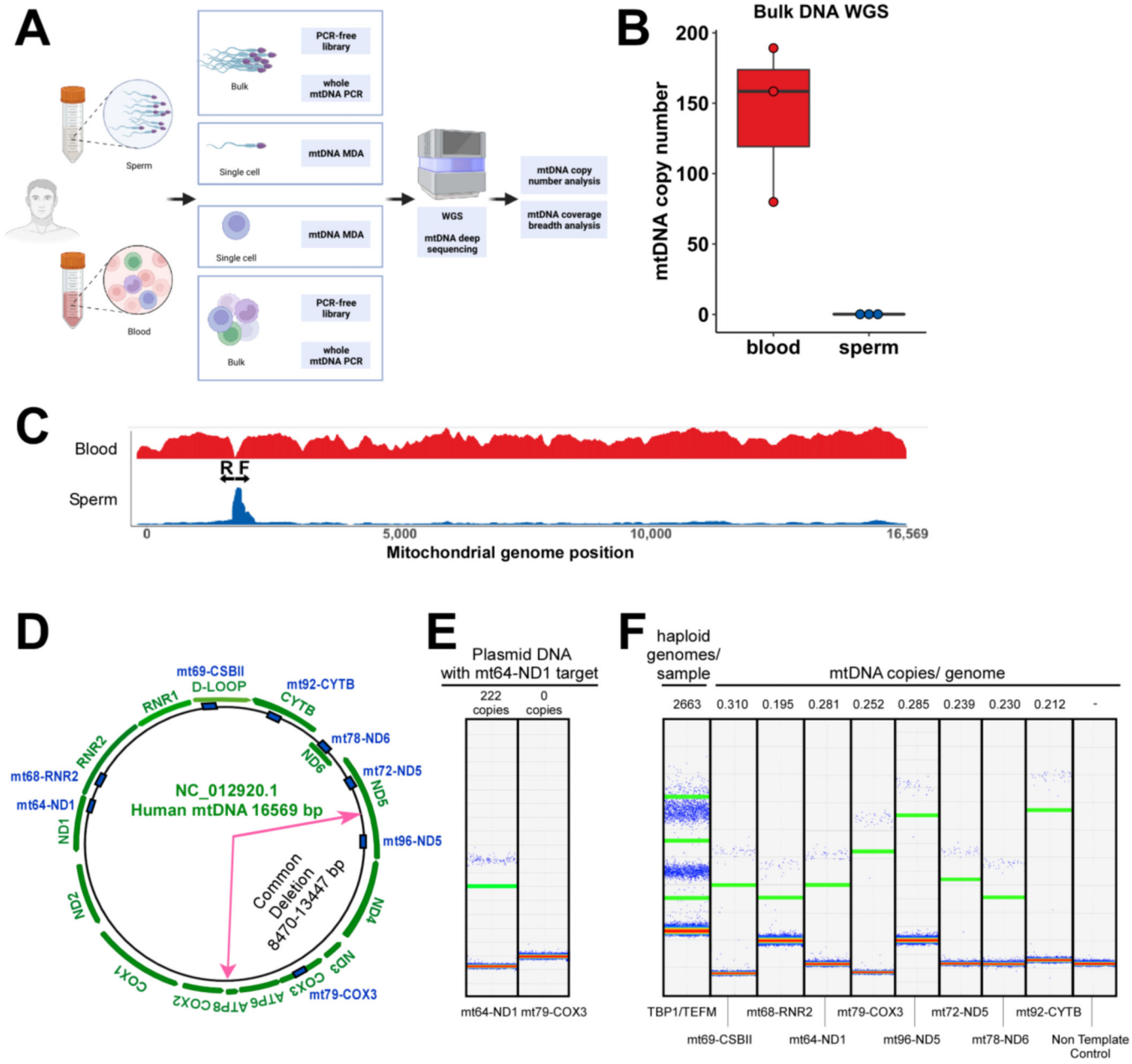

Extended Data Fig. 1. Mitochondria of human spermatozoa contain no mtDNA.

A. Schematics of the mtDNA copy number assessment in sperm cells using Whole Genome Sequencing (WGS). **B.** Box plots of mtDNA copy number (mtDNA/per cell) analysis in bulk spermatozoa and blood samples (n=3); n represents a biologically independent number of samples. Center line, median; box bounds, 25th and 75th percentiles; whiskers, minimum to maximum within 1.5 interquartile range; data points outside whiskers, outliers. **C.** Illustration of a mitochondrial genome coverage breadth in bulk blood cells (top) and spermatozoa (bottom) sample (donor 2) enriched for mtDNA using long-range PCR amplifying full-length mtDNA in one reaction. A peak in the read density observed in the

region of priming of the PCR primers (black arrows, position ~2,000 nt) in spermatozoa but not in the blood cells likely reflects the presence of degraded mtDNA molecules. **D.** Schematic of human mtDNA showing the location of sequences targeted by different primer pairs. Pink arrows indicate the mtDNA common deletion region. The name and location of the amplicons are shown in blue. **E.** Representative one-dimension droplet scatter plot illustrating the accuracy of ddPCR in mtDNA detection. The pJET plasmid containing only the mt64-ND1 target mtDNA fragment was used; amplification was performed using mt64-ND1 and mt79-COX3 primers. **F**. Representative one-dimension droplet scatter plots were obtained using different primer pairs after ddPCR of DNA in the same spermatozoa sample. Blue dots above the green line indicate amplicon-positive droplets. The absolute mtDNA copy number is given for each primer pair at the top of the panel.

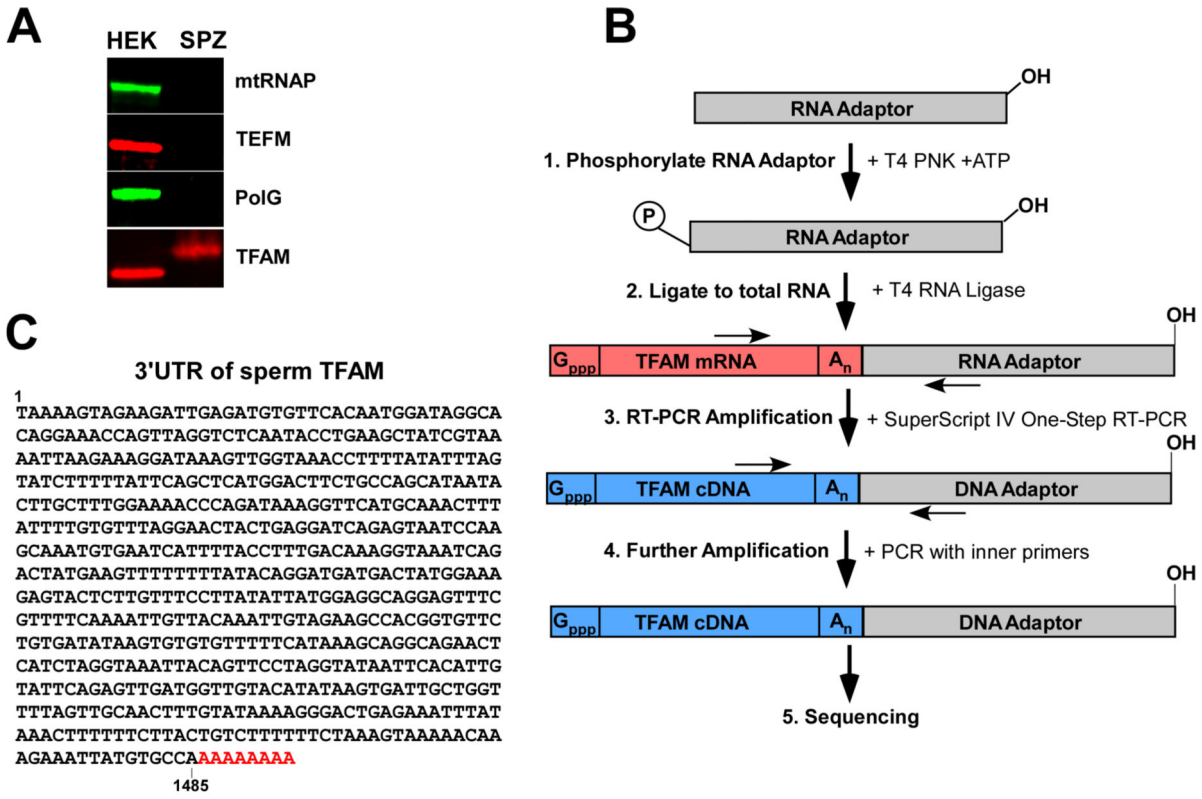

Extended Data Fig. 2. Mapping of the UTRs of the sperm TFAM isoform.

A. Western blot analysis of the proteins indicated in mitochondria of HEK cells and spermatozoa (SPZ). **B.** Schematics of the RACE experiment. **C.** The sequence of the 3' UTR of the sperm TFAM cDNA **D.** Schematic illustration of polyadenylation of the TFAM mRNA in somatic cells. PAS – polyadenylation signal. **E.** Schematic illustration of polyadenylation of the TFAM mRNA in sperm cells. Putative polyadenylation signal (PAS) and UGUAN elements are indicated.

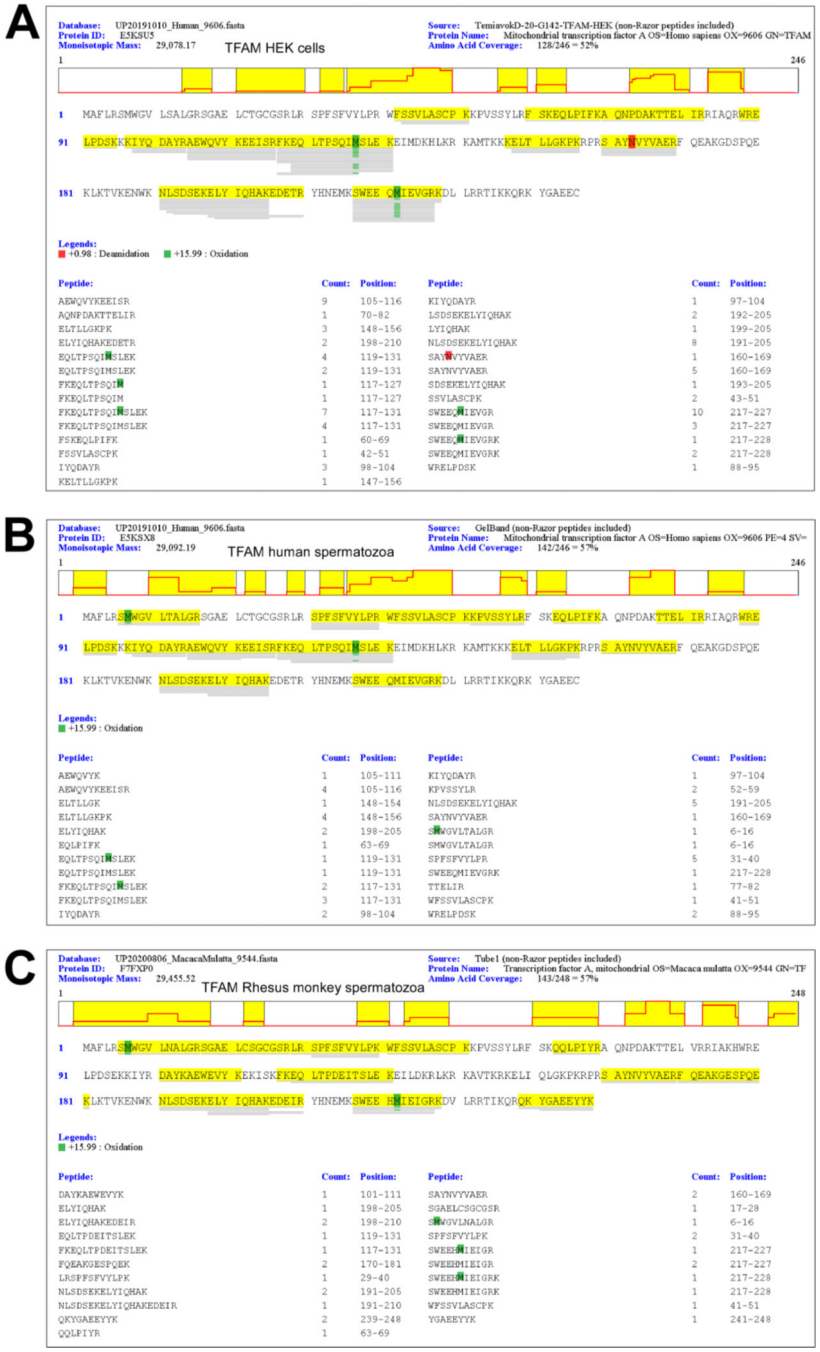

Extended Data Fig. 3. Identification of TFAM peptides by LC-MS/MS analysis in HEK cells (A), human (B), and Rhesus monkey (C) spermatozoa.

Peptide search was done using MaxQuant. Note that the SGAELCSGCGSR peptide was identified in the human sperm TFAM sample using pFind and, therefore, not shown in panel B.

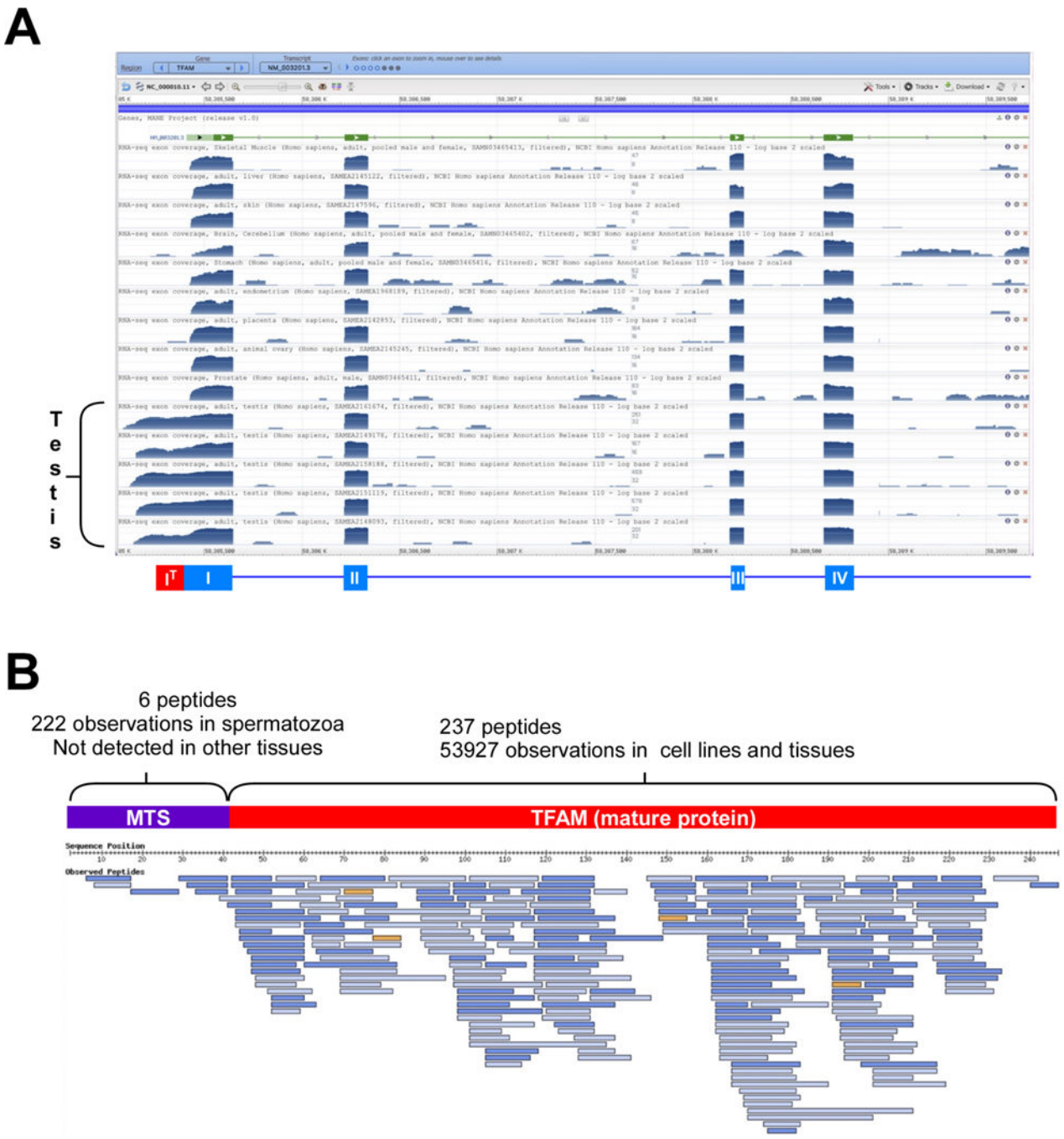

Extended Data Fig. 4. Pattern of TFAM expression in different human tissues.

A. Exon I^T is detected only in mRNA ftom testis. Histograms of RNA-seq data from 10 different tissues have been visualized using the Genome Data Viewer (NCBI). The schematic of the TFAM pre-mRNA is shown below the histograms. **B.** TFAM peptides matching the mitochondrial pre-sequence are not detected in somatic tissues. The uniquely-mapping protein-calling peptides are shown as blue bars and multi-mapping and non-tryptic peptides are yellow bars. Light blue, 1–4 observations. Dark blue, five or more observations.

Proteomic data were obtained from 1099 proteomic experiments. Source: Peptide Atlas (db.systemsbiology.net).

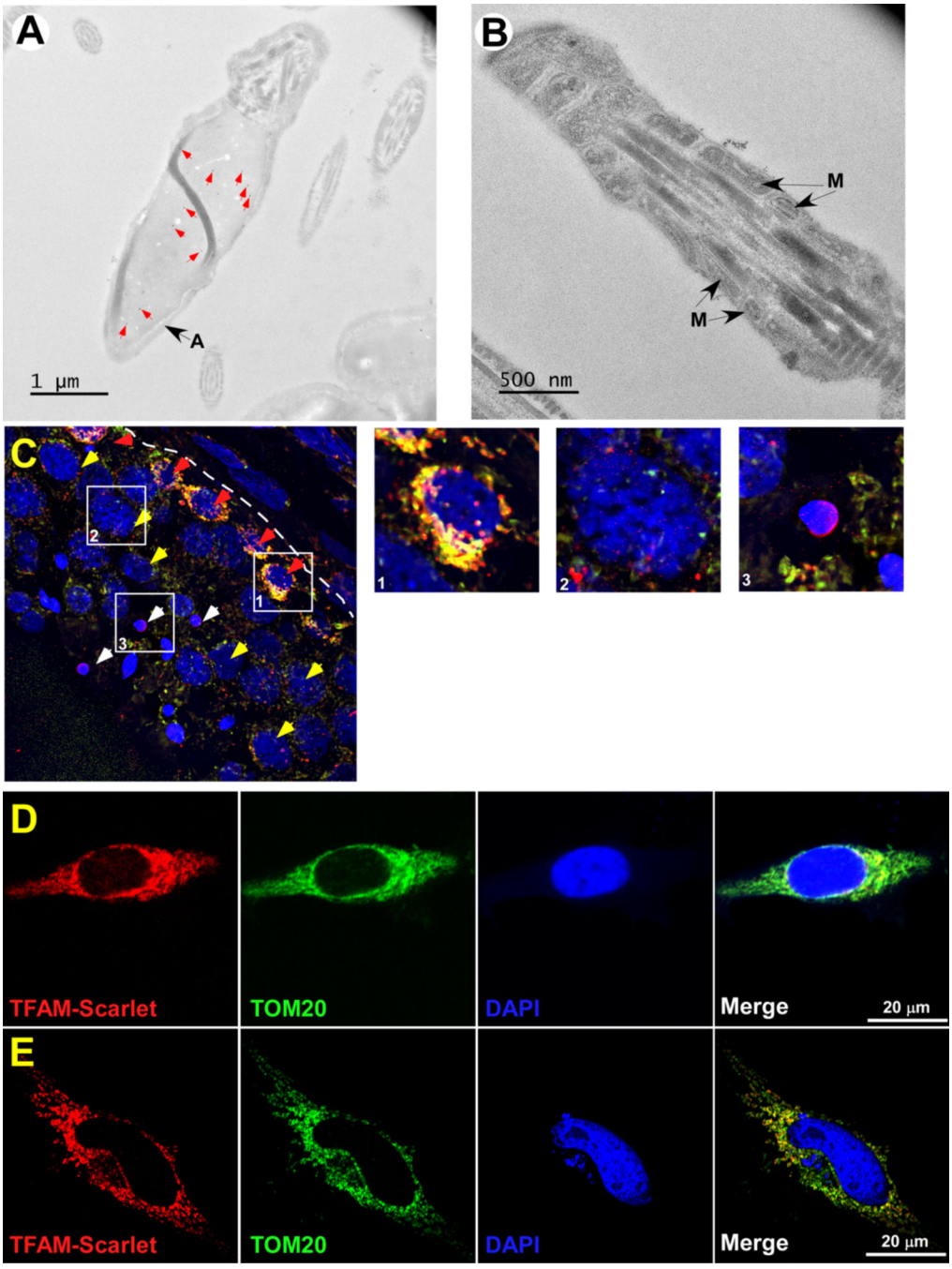

Extended Data Fig. 5. TFAM localization in spermatozoa and somatic cells.

A. Cryo immunogold electron microscopy of spermatozoa head. Red arrows indicate gold particles. A - acrosome. **B**. Cryo immunogold electron microscopy of spermatozoon midpiece. M- mitochondria. **C.** Staining of human testicular tissue. Merge image. Red-staining with anti-TFAM antibody, blue- DAPI, green -staining with anti-TOM20 antibody.

Red arrows - spermatogonia, yellow – spermatocytes, white – spermatids. The basement membrane is indicated by a dashed line, L- seminiferous tubule lumen. Close-up images of spermatogonia (1), spermatocytes (2) and spermatids (3) correspond to the white squares indicated. **D.** Over-expressed TFAM having the somatic 5' and 3' UTRs shows mitochondrial localization in HeLa cells. **E.** Overexpressed TFAM lacking UTRs shows mitochondrial localization in HeLa cells

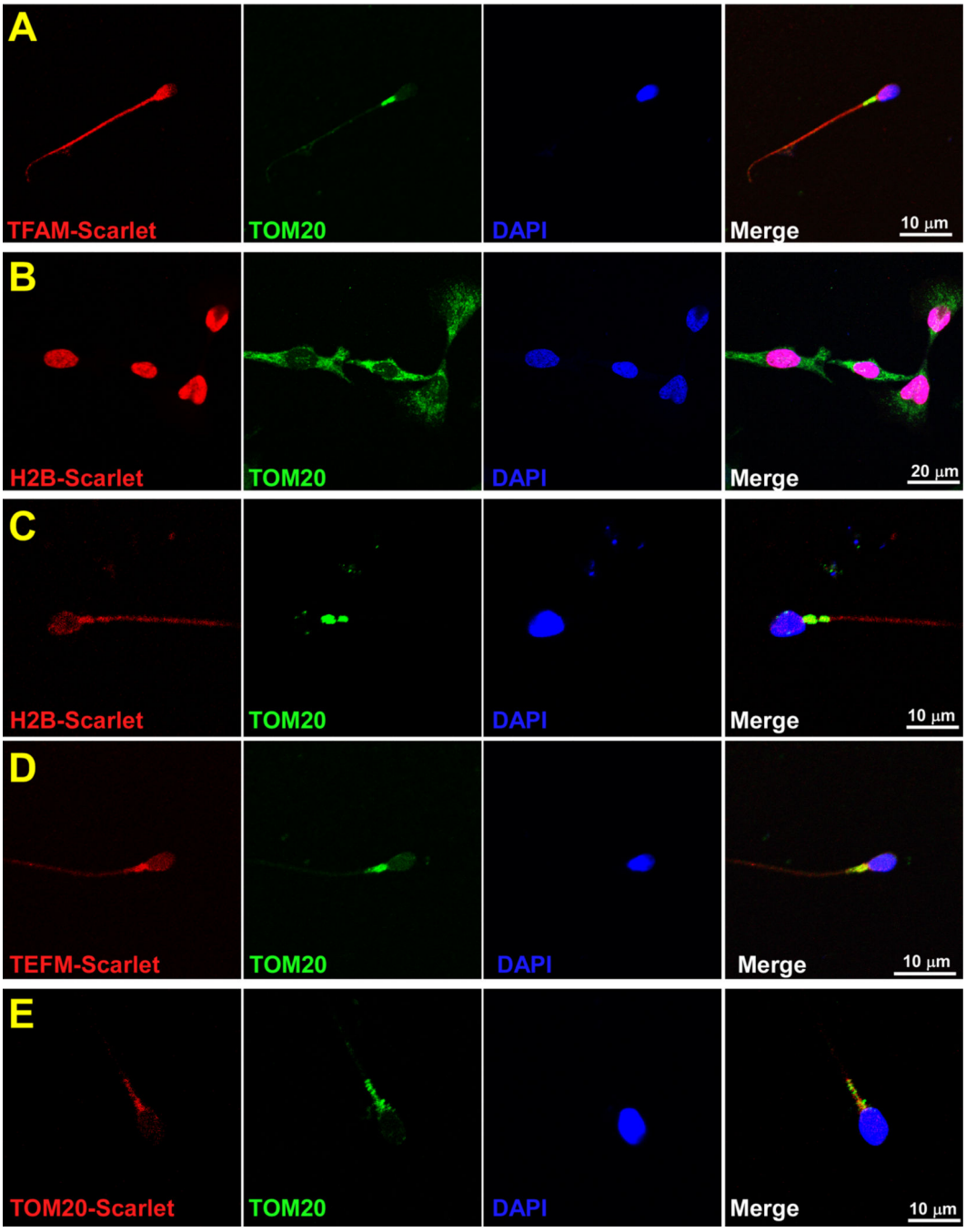

Extended Data Fig. 6. Expression of TFAM, H2B, TEFM, and TOM20 in somatic cells and mature spermatozoa.

A. Over-expression of TFAM mRNA having sperm 3’ and 5’ UTR regions result in cytoplasmic localization of this protein in spermatozoa. **B.** Over-expression of H2B in HeLa cells shows nuclear localization. **C.** Over-expression of H2B in sperm cells results in cytoplasmic localization. **D.** Over-expression of TEFM shows mitochondrial localization in spermatozoa. **E.** Over-expression of TOM20 results in mitochondrial localization in spermatozoa

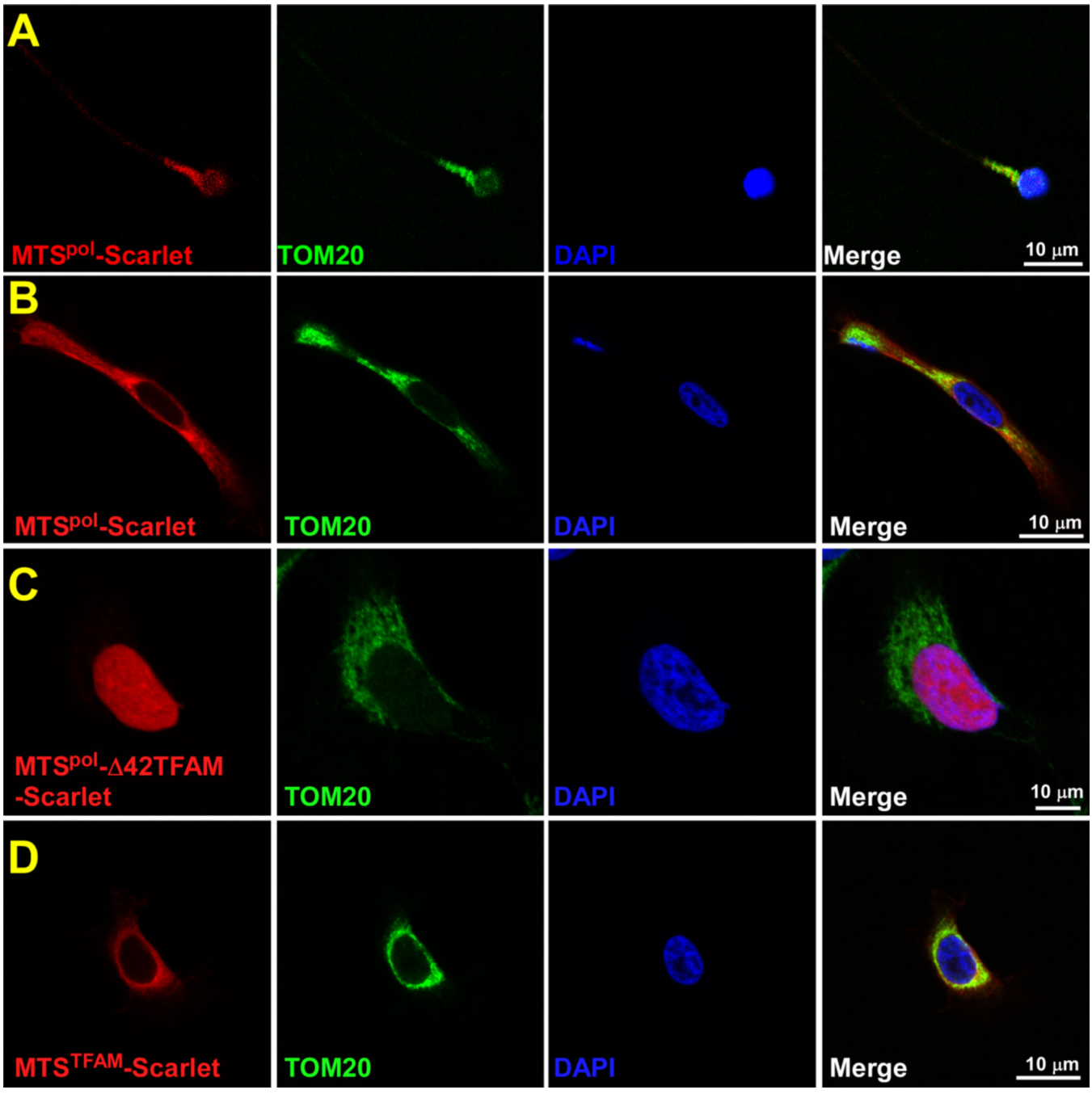

Extended Data Fig. 7. Trafficking of the TFAM variants in HeLa cells.

A. MTS^{pol}-mScarlet protein is localized to the sperm mitochondria.
B. MTS^{pol}-mScarlet is localized to mitochondria in HeLa cells.
C. MTS^{pol}-Δ42TFAM is localized to the nucleus of HeLa cells.
D. MTS^{TFAM}-Scarlet is localized to mitochondria in HeLa cells

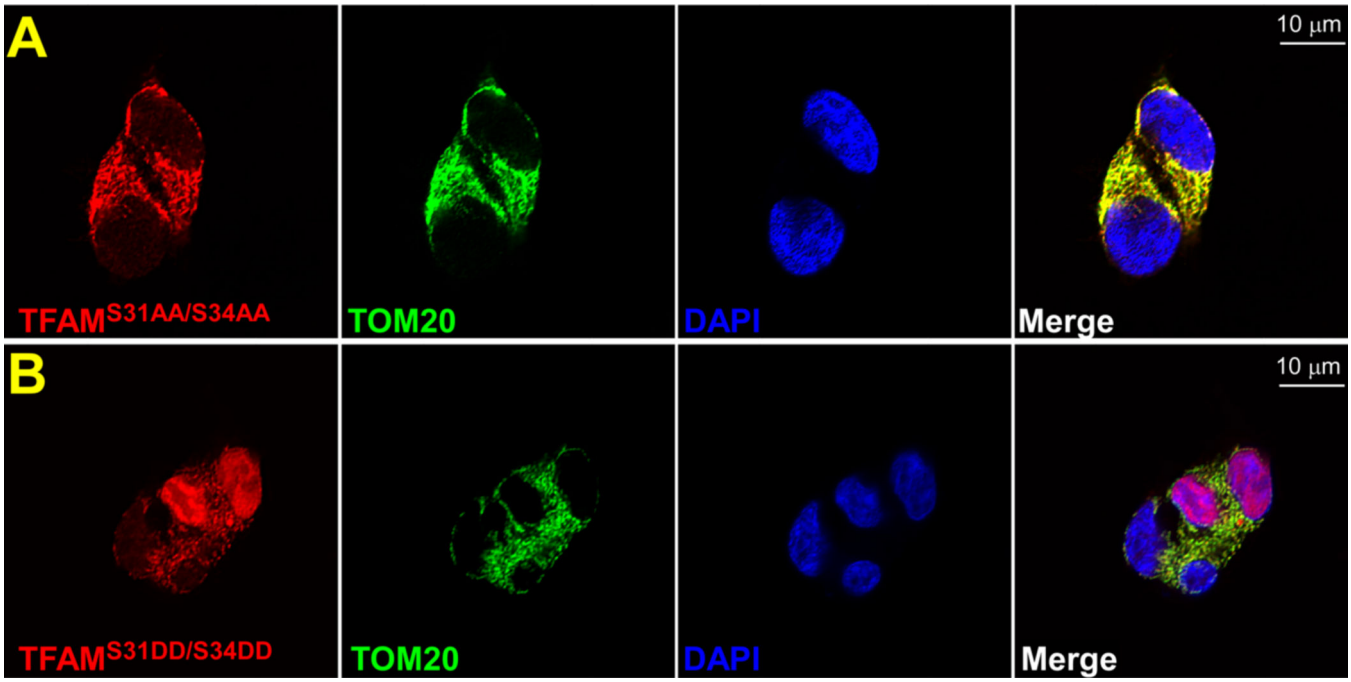

Extended Data Fig. 8. Expression of the phosphomimicking TFAM variant in HEK293 cells.
A. TFAM$^{S31AA/S34AA}$-mScarlet protein is localized to the mitochondria of HEK293 cells.
B. TFAM$^{S31DD/S34DD}$-mScarlet protein is localized to the nucleus of HEK293 cells.

Extended Data Table 1.

MtDNA copy number (CN) analysis of the blood and spermatozoa samples by Whole Genome Sequencing.

Research Donor	Origin	DNA	Mean Autosome Coverage Depth	Mean MtDNA Coverage Depth	Autosome CN	MtDNA CN
D1	Blood	Bulk	2.7	256.2	2	189.15
D1	Sperm	Bulk	3.6	0.6	1	0.17
D2	Blood	Bulk	4.2	332.1	2	158.43
D2	Sperm	Bulk	4.5	0.7	1	0.16
D4	Blood	Bulk	4.7	188.4	2	79.86
D4	Sperm	Bulk	4.2	0.4	1	0.10

Extended Data Table 2.

Deep sequencing of enriched mtDNA from the blood and spermatozoa samples.

Research Donor	Origin	DNA	Genome	Number of Genomic Reads	MtDNA Coverage Breadth (%)	Mean Coverage Depth
D1	Blood	Bulk, PCR-based whole mtDNA enrichment	Mt	2,745,115	100	22654
D1	Sperm	Bulk, PCR-based whole mtDNA enrichment	Mt	85,853	100	618
D2	Blood	Bulk, PCR-based whole mtDNA enrichment	Mt	3,174,670	100	27274
D2	Sperm	Bulk, PCR-based whole mtDNA enrichment	Mt	430,159	100	3038
D3	Blood	Bulk, PCR-based whole mtDNA enrichment	Mt	2,795,408	100	22103
D3	Sperm	Bulk, PCR-based whole mtDNA enrichment	Mt	630,113	100	4498
D4	Blood	Bulk, PCR-based whole mtDNA enrichment	Mt	1,696,055	100	13412
D4	Sperm	Bulk, PCR-based whole mtDNA enrichment	Mt	439,774	100	3737

Extended Data Table 3.

Oligonucleotides used in the study.

Name of oligonucleotide	5’−3’ Sequence
TFAM: Cloning into pWPXL	
TFAM ORF END (FWD)	AAAATATGGTGCTGAGGAGTGTTAA
TFAM 3’ Mt UTR (REV)	TGTGTTTCAACAAACTTTATTTATGAACAC
Restriction site: Mt 3’ UTR (FWD)	CCGGAATTCAAGTAG AAGATTGAGATGTGTTCAC
Restriction site: Mt 3’ UTR (REV)	GGAATTCCATATG TGTGTTTCAACAAACTTTATT TATGAACAC
Megaprimer: Nuclear 3’ UTR (FWD)	CGGCATGGACGAGCTGTACAAGTAAAAGTAGAAGA TTGAGATGTGTTCAC
Megaprimer: Nuclear 3’ UTR (REV)	ATCATATGACTAGTCCCGGGAATTCGAGAGAAAAT AATTCAGAAAAAAATAAAATTCC
Megaprimer: Mt 5’ UTR (FWD)	CCTCGAGGTTTAAACTACGGGATCCCCTCGCTAGT GGCGGGCATGATAACACA
Megaprimer: Nuclear 5’ UTR (FWD)	CCTCGAGGTTTAAACTACGGGATCCGGGGTGAGGC CGCCGCCG
Megaprimer: Mt/Nuclear 5’ UTR (REV)	CCCACATGCTTCGGAGAAACGCCAT
Mutagenesis: Del42 TFAM-mScarlet with Mt 5’ and 3’ UTRs (FWD)	CATCCACCGGAGCGATGTCATCTGTCTTGGCAAGT TG
Mutagenesis: Del42 TFAM-mScarlet with Mt 5’ and 3’ UTRs (REV)	CAACTTGCCAAGACAGATGACATCGCTCCGGTGGA TG
Megaprimer: Kozak mtRNAP MTS (FWD)	GCCTCGAGGTTTAAACTACCATGTCGGCACTTTGC
Megaprimer: MTS RNAP TFAM (REV)	GGACAACTTGCCAAGACAGATGAGGCGGACGAGCT CCTCC
Mutagenesis: MTS-Del TFAM Scarlet (FWD)	CGAGGTGGTTTTCATCTGTCAGCAAGGGCGAGGCA GTGAT

Name of oligonucleotide	5’−3’ Sequence
Mutagenesis: MTS-Del TFAM Scarlet (REV)	ATCACTGCCTCGCCCTTGCTGACAGATGAAAACCA CCTCG
Mutagenesis: TFAM S31D S34D (FWD)	GCTGTGGAAGTCGACTGCGCGACCCCTTCGATTTT GTGTATTTACCGAGGTG
Mutagenesis: TFAM S31D S34D (REV)	CACCTCGGTAAATACACAAAATCGAAGGGGTCGCG CAGTCGACTTCCACAGC
Mutagenesis: TFAM S31A P32A S34A F35A (FWD), $TFAM^{S31AA/S34AA}$	GTGGAAGTCGACTGCGCGCCGCCTTCGCTGCTGTG TATTTACCGAGG
Mutagenesis: TFAM S31A P32A S34A F35A (REV), $TFAM^{S31AA/S34AA}$	CCTCGGTAAATACACAGCAGCGAAGGCGGCGCGCA GTCGACTTCCAC
Mutagenesis: TFAM S31D P32D S34D F35D(FWD), $TFAM^{S31DD/S34DD}$	GCTGTGGAAGTCGACTGCGCGACGACTTCGATGAT GTGTATTTACCGAGG
Mutagenesis: TFAM S31A P32A S34A F35A(REV), $TFAM^{S31DD/S34DD}$	CCTCGGTAAATACACATCATCGAAGTCGTCGCGCA GTCGACTTCCACAGC
TFAM: Cloning into pET3a	
Restriction site: Nde_TFAM (FWD)	GGAATTCCATATGGCGTTTCTCCGAAGCATGTGGG
Restriction site: BamHI_mScarlet (REV)	CGCGGATCCTCTTACTTGTACAGCTCGTCCATGC
Mutagenesis: HisTFAMscarletPET (FWD)	GCATGGACGAGCTGTACAAGCATCACCATCACCAT CACTAAGAGGATCCGGCTGC
Mutagensis: HisTFAMscarletPET (REV)	GCAGCCGGATCCTCTTAGTGATGGTGATGGTGATG CTTGTACAGCTCGTCCATGC
Protein Controls: Cloning into pWPXL	
TOM20 FWD	ATGGTGGGTCGGAACAG
TOM20 REV	TTCCACATCATCTTCAGCCA
Megaprimer: TOM20 pt7blue (FWD)	CGAGGTTTAAACTACGGGATCCATGGTGGG TCGGAACAG
Megaprimer: TOM20 pt7blue (REV)	CCTTGCTCACAGAACCACCACCACCTTCCACATCA TCTTCAGCCA
Megaprimer: H2B Type 1a (FWD)	CGAGGTTTAAACTACGGGATCCATGCCGGAGGTGT CATCT
Megaprimer: H2B Type 1a (REV)	CCTTGCTCACAGAACCACCACCACCCTTGGAGCTG GTGTACTTAG
Northern Blot	
TFAM_Exon 4	TCTTCTTTATATACCTGCCACTCCGCCCTA
18S rRNA	GCCCCGCGGGACACTCA
5’ & 3’ RLM-RACE, RT-PCR	
RNA Adaptor (Ambion)	GCUGAUGGCGAUGAAUGAACACUGCGUUUGCUGGC UUUGAUGAAA
Adaptor_Inner (REV)	GTTCATTCATCGCCATCAGC
Adaptor_Outer (REV)	TTTCATCAAAGCCAGCAAACGC
Adaptor_Inner (FWD) (Ambion)	CGCGGATCCGAACACTGCGTTTGCTGGCTTTGATG
Adaptor_Outer (FWD) (Ambion)	GCTGATGGCGATGAATGAACACTG
TFAM_Exon 3 (REV)	CCCTCCAACGCTGGGCAATT
TFAM_Exon 2 (REV)	CCAAGACAGATGAAAACCACC
TFAM_3’ UTR (FWD)	AAGCCACGGTGTTCTGTGAT
TFAM_3’ UTR Inner (FWD)	GCAGGCAGAACTCATCTAGG
TFAM_Exon 1T (FWD)	GGATTGCGGTTTCCCTTCAT

Name of oligonucleotide	5’−3’ Sequence
ddPCR: MtDNA	
mt92-CYTB (H-strand)	GGGTATAATTGTCTGGGTCGCC
mt92-CYTB (L-strand)	AGACGCCCTCGGCTTACTTC
mt64-ND1 (H-strand)	AGATGTGGCGGGTTTTAGGG
mt64-ND1 (L-strand)	ACTACAACCCTTCGCTGACG
mt69-CSBII (H-strand)	TGGTTAGGCTGGTGTTAGGG
mt69-CSBII (L-strand)	CTGGCCACAGCACTTAAACAC
mt-68-RNR2 (H-strand)	CCTTTCGTACAGGGAGGAATTTG
mt-68-RNR2 (L-strand)	TCTGAGTTCAGACCGGAGTA
mt79-COX3 (H-strand)	GCCAATAATGACGTGAAGTCCG
mt79-COX3 (L-strand)	CTTCACCATTTCCGACGGC
mt96-ND5 (H-strand)	GGTGAGGCTTGGATTAGCGT
mt96-ND5 (L-strand)	ATCGGTTTCATCCTCGCCTT
mt72-ND5 (H-strand)	GGCTGTGAGTTTTAGGTAGAGGG
mt72-ND5 (L-strand)	CTCATTACTAACAACATTTCCCCCG
mt78-ND6 (H-strand)	GGTCAGGGGTTGAGGTCTTG
mt78-ND6 (L-strand)	ACTCTTTCACCCACAGCACC
ddPCR: Nuclear DNA	
TEFM88	GTGACTCCCGGACTAGTGGA
TEFM88	GATGGGAAGAACACCCGAGG
TBP73	CACCACAGCTCTTCCACTCA
TBP73	GGGGAGGGATACAGTGGAGT
Long-range PCR	
F	GGACACTAGGAAAAAACCTTGTAGAGAGAG
R	AAAGAGCTGTTCCTCTTTGGACTAACA

Extended Data Table 4.

Plasmids generated during the study.

Name of the construct	Parent plasmid
TFAM-mScarlet_pWPXL	pWPXL (Addgene ref #12257)
3’mitoUTR_TFAM-mScarlet_pWPXL	TFAM-mScarlet_pWPXL
5’mitoUTR_TFAM-mScarlet_pWPXL	TFAM-mScarlet_pWPXL
3’5’mitoUTR_TFAM-mScarlet_pWPXL	3’mitoUTR_TFAM-mScarlet_pWPXL
3’nuclUTR_TFAM-mScarlet_pWPXL	TFAM-mScarlet_pWPXL
5’nuclUTR_TFAM-mScarlet_pWPXL	TFAM-mScarlet_pWPXL
3’5’nuclUTR_TFAM-mScarlet_pWPXL	3’nuclUTR_TFAM-mScarlet_pWPXL
Δ42TFAM-mScarlet_pWPXL	3’5’mitoUTR_TFAM-mScarlet_pWPXL
TOM20-mScarlet_pWPXL	TFAM-mScarlet_pWPXL

Name of the construct	Parent plasmid
H2B-mScarlet_pWPXL	TFAM-mScarlet_pWPXL
MTS^{TFAM}mScarlet_pWPXL	TFAM-mScarlet_pWPXL
MTS^{pol}Δ42TFAM-mScarlet_pWPXL	TFAM-mScarlet_pWPXL
MTS^{pol}-mScarlet_pWPXL	mtRNAP_pWPXL
mScarlet_pWPXL	TFAM-mScarlet_pWPXL
S31A/S34A_TFAM-mScarlet_pWPXL	TFAM-mScarlet_pWPXL
TFAM-mScarlet_C-his6	pcDNA-TFAM-mScarlet (Addgene ref # 129573)
$TFAM^{S31AA/S34AA}$	TFAM-mScarlet_pWPXL
$TFAM^{S31DD/S34DD}$	TFAM-mScarlet_pWPXL

Supplementary Material

Refer to Web version on PubMed Central for supplementary material.

Acknowledgments:

We thank NYULH DART Microscopy Laboratory, Alice Liang, Chris Petzold, and Kristen Dancel-Manning for consultation and assistance with TEM work; this core is partially funded by NYU Cancer Center Support Grant NIH/NCI P30CA016087. The authors are indebted to Crystal Van Dyken, David Battaglia, and the Oregon National Primate Research Center staff, OHSU Reproductive Endocrinology, and IVF clinic for their expertise and services in obtaining monkey and human gametes for this study. We are grateful to all study participants for sperm and blood donations and to Ying Li and Daniel Frana from the OHSU Center for Embryonic Cell and Gene Therapy, and to Brian Sereda and other staff members from the OHSU Fertility Consultants and Andrology Division in the Department of Obstetrics and Gynecology for their assistance in procurement and preparation of sperm and tissue donations. We thank Thomas Jefferson University BioImaging facility and Dr. Maria Covarrubias for help with confocal microscopy experiments. Dr. Michael Anikin and William T. McAllister are acknowledged for the critical reading of the manuscript and fruitful discussion.

Data Availability

Source data are provided with this paper. The mass spectrometry proteomics data have been deposited into the MassIVE (massive.ucsd.edu) and ProteomeXchange (proteomexchange.org) data repository with the accession number MSV000092433 and PXD043765, respectively.

Mitochondrial and nuclear DNA sequencing read counts, extracted from the whole-genome sequencing datasets and used for inference of mitochondrial DNA copy number, are included in Extended Data Table 1. However, whole-genome sequencing of nuclear and mitochondrial DNA datasets themselves are not central to the research findings and conclusions presented in this manuscript. In accordance with international laws and OHSU IRB regulations and the terms of the consent signed by the research participants, protecting the anonymity of research participants is one of the key ethical requirements for our clinical research. Since the genetic identity of gamete donors can be revealed by whole-genome sequencing information, these datasets cannot be publicly uploaded or shared outside of the OHSU network. Our priority is to protect the privacy of our participants while facilitating responsible and controlled access to the research data for legitimate research purposes. Therefore, we are willing to provide this information on a case-by-case basis upon approval

by the OHSU IRB and Research Integrity chairs. Approved requestors will be directed to an OHSU compliance officer to initiate a Non-Disclosure Agreement, ensuring the confidentiality of our research participants. Upon successful approval, the requestor will be escorted by a team member at all times and granted access to an OHSU computer in a shared office where they can access and review the whole-genome sequencing datasets. All requests should be initiated with OHSU Research Integrity and will follow their established process, which may take upwards of 3–6 months. To request access, interested parties should contact Kara Drolet, Associate VP, ORIO, at irb@ohsu.edu.

Code availability statement

Scripts for Picard tools (v2.26.9) used on Genome Analysis Toolkit (GATK) for preprocessing raw sequencing reads to produce BAM were available in the following GitHub repository: http://broadinstitute.github.io/picard.

References

1. Ankel-Simons F & Cummins JM Misconceptions about mitochondria and mammalian fertilization: implications for theories on human evolution. Proc Natl Acad Sci U S A 93, 13859–63 (1996). [PubMed: 8943026]
2. Wallace DC Why do we still have a maternally inherited mitochondrial DNA? Insights from evolutionary medicine. Annu Rev Biochem 76, 781–821 (2007). [PubMed: 17506638]
3. Sutovsky P et al. Ubiquitinated sperm mitochondria, selective proteolysis, and the regulation of mitochondrial inheritance in mammalian embryos. Biol Reprod 63, 582–90 (2000). [PubMed: 10906068]
4. Sato M & Sato K Degradation of paternal mitochondria by fertilization-triggered autophagy in C. elegans embryos. Science 334, 1141–4 (2011). [PubMed: 21998252]
5. Luo SM et al. Unique insights into maternal mitochondrial inheritance in mice. Proc Natl Acad Sci U S A 110, 13038–43 (2013). [PubMed: 23878233]
6. Boudoures AL et al. Obesity-exposed oocytes accumulate and transmit damaged mitochondria due to an inability to activate mitophagy. Dev Biol 426, 126–138 (2017). [PubMed: 28438607]
7. Birky CW Jr. Uniparental inheritance of mitochondrial and chloroplast genes: mechanisms and evolution. Proc Natl Acad Sci U S A 92, 11331–8 (1995). [PubMed: 8524780]
8. Hoekstra RF Evolutionary origin and consequences of uniparental mitochondrial inheritance. Hum Reprod 15 Suppl 2, 102–11 (2000). [PubMed: 11041518]
9. Havird JC et al. Selfish Mitonuclear Conflict. Curr Biol 29, R496–R511 (2019). [PubMed: 31163164]
10. Sharpley MS et al. Heteroplasmy of mouse mtDNA is genetically unstable and results in altered behavior and cognition. Cell 151, 333–343 (2012). [PubMed: 23063123]
11. DeLuca SZ & O'Farrell PH Barriers to male transmission of mitochondrial DNA in sperm development. Dev Cell 22, 660–8 (2012). [PubMed: 22421049]
12. Rantanen A & Larsson NG Regulation of mitochondrial DNA copy number during spermatogenesis. Hum Reprod 15 Suppl 2, 86–91 (2000).
13. Manfredi G, Thyagarajan D, Papadopoulou LC, Pallotti F & Schon EA The fate of human sperm-derived mtDNA in somatic cells. Am J Hum Genet 61, 953–60 (1997). [PubMed: 9382109]
14. Diez-Sanchez C et al. Mitochondrial DNA content of human spermatozoa. Biol Reprod 68, 180–5 (2003). [PubMed: 12493711]
15. Boguenet M et al. Mitochondrial DNA content reduction in the most fertile spermatozoa is accompanied by increased mitochondrial DNA rearrangement. Hum Reprod 37, 669–679 (2022). [PubMed: 35150574]

16. Podlesniy P & Trullas R Absolute measurement of gene transcripts with Selfie-digital PCR. Sci Rep 7, 8328 (2017). [PubMed: 28827685]
17. Giles RE, Blanc H, Cann HM & Wallace DC Maternal inheritance of human mitochondrial DNA. Proc Natl Acad Sci U S A 77, 6715–9 (1980). [PubMed: 6256757]
18. Wang G et al. In-depth proteomic analysis of the human sperm reveals complex protein compositions. J Proteomics 79, 114–22 (2013). [PubMed: 23268119]
19. Baker MA et al. Identification of gene products present in Triton X-100 soluble and insoluble fractions of human spermatozoa lysates using LC-MS/MS analysis. Proteomics Clin Appl 1, 524–32 (2007). [PubMed: 21136703]
20. Castillo J et al. Proteomic Changes in Human Sperm During Sequential in vitro Capacitation and Acrosome Reaction. Front Cell Dev Biol 7, 295 (2019). [PubMed: 31824947]
21. Larsson NG, Oldfors A, Garman JD, Barsh GS & Clayton DA Down-regulation of mitochondrial transcription factor A during spermatogenesis in humans. Hum Mol Genet 6, 185–91 (1997). [PubMed: 9063738]
22. Larsson NG et al. Mitochondrial transcription factor A is necessary for mtDNA maintenance and embryogenesis in mice. Nat Genet 18, 231–6 (1998). [PubMed: 9500544]
23. Ekstrand MI et al. Mitochondrial transcription factor A regulates mtDNA copy number in mammals. Hum Mol Genet 13, 935–44 (2004). [PubMed: 15016765]
24. Otten ABC et al. Tfam Knockdown Results in Reduction of mtDNA Copy Number, OXPHOS Deficiency and Abnormalities in Zebrafish Embryos. Front Cell Dev Biol 8, 381 (2020).
25. Matsushima Y et al. Functional domains of chicken mitochondrial transcription factor A for the maintenance of mitochondrial DNA copy number in lymphoma cell line DT40. J Biol Chem 278, 31149–58 (2003). [PubMed: 12759347]
26. Kanki T et al. Architectural role of mitochondrial transcription factor A in maintenance of human mitochondrial DNA. Mol Cell Biol 24, 9823–34 (2004). [PubMed: 15509786]
27. Wang LJ, Hsu T, Lin HL & Fu CY Modulation of mitochondrial nucleoid structure during aging and by mtDNA content in Drosophila. Biol Open 10(2021).
28. Saint-Georges Y et al. Yeast mitochondrial biogenesis: a role for the PUF RNA-binding protein Puf3p in mRNA localization. PLoS One 3, e2293 (2008). [PubMed: 18523582]
29. Kosugi S, Hasebe M, Tomita M & Yanagawa H Systematic identification of cell cycle-dependent yeast nucleocytoplasmic shuttling proteins by prediction of composite motifs. Proc Natl Acad Sci U S A 106, 10171–6 (2009). [PubMed: 19520826]
30. Miller D, Brinkworth M & Iles D Paternal DNA packaging in spermatozoa: more than the sum of its parts? DNA, histones, protamines and epigenetics. Reproduction 139, 287–301 (2010). [PubMed: 19759174]
31. Urizar-Arenaza I et al. Phosphoproteomic and Functional Analyses Reveal Sperm-specific Protein Changes Downstream of Kappa Opioid Receptor in Human Spermatozoa. Mol Cell Proteomics 18, S118–S131 (2019). [PubMed: 30622161]
32. Wiedemann N & Pfanner N Mitochondrial Machineries for Protein Import and Assembly. Annu Rev Biochem 86, 685–714 (2017). [PubMed: 28301740]
33. Lee J, O'Neill RC, Park MW, Gravel M & Braun PE Mitochondrial localization of CNP2 is regulated by phosphorylation of the N-terminal targeting signal by PKC: implications of a mitochondrial function for CNP2 in glial and non-glial cells. Mol Cell Neurosci 31, 446–62 (2006). [PubMed: 16343930]
34. Law YS et al. Phosphorylation and Dephosphorylation of the Presequence of Precursor MULTIPLE ORGANELLAR RNA EDITING FACTOR3 during Import into Mitochondria from Arabidopsis. Plant Physiol 169, 1344–55 (2015). [PubMed: 26304849]
35. Niemi NM et al. Pptc7 is an essential phosphatase for promoting mammalian mitochondrial metabolism and biogenesis. Nat Commun 10, 3197 (2019). [PubMed: 31324765]
36. Sutovsky P et al. Ubiquitin tag for sperm mitochondria. Nature 402, 371–2 (1999). [PubMed: 10586873]
37. Lee K et al. Hepatic Mitochondrial Defects in a Nonalcoholic Fatty Liver Disease Mouse Model Are Associated with Increased Degradation of Oxidative Phosphorylation Subunits. Mol Cell Proteomics 17, 2371–2386 (2018). [PubMed: 30171159]

38. Karunadharma PP et al. Respiratory chain protein turnover rates in mice are highly heterogeneous but strikingly conserved across tissues, ages, and treatments. FASEB J 29, 3582–92 (2015). [PubMed: 25977255]
39. Piomboni P, Focarelli R, Stendardi A, Ferramosca A & Zara V The role of mitochondria in energy production for human sperm motility. Int J Androl 35, 109–24 (2012). [PubMed: 21950496]
40. Ruiz-Pesini E et al. Correlation of sperm motility with mitochondrial enzymatic activities. Clin Chem 44, 1616–20 (1998). [PubMed: 9702947]
41. Wolf DP, Mitalipov PA & Mitalipov SM Principles of and strategies for germline gene therapy. Nat Med 25, 890–897 (2019). [PubMed: 31160821]
42. Ma H et al. Germline transmission of donor, maternal and paternal mtDNA in primates. Hum Reprod 36, 493–505 (2021). 10.1093/humrep/deaa308 [PubMed: 33289786]
43. Podlesniy P et al. Accumulation of mitochondrial 7S DNA in idiopathic and LRRK2 associated Parkinson's disease. EBioMedicine 48, 554–567 (2019). 10.1016/j.ebiom.2019.09.015 [PubMed: 31631040]
44. DePristo MA et al. A framework for variation discovery and genotyping using next-generation DNA sequencing data. Nat Genet 43, 491–498 (2011). 10.1038/ng.806 [PubMed: 21478889]
45. Li H et al. The Sequence Alignment/Map format and SAMtools. Bioinformatics 25, 2078–2079 (2009). 10.1093/bioinformatics/btp352 [PubMed: 19505943]
46. Robinson JT et al. Integrative genomics viewer. Nat Biotechnol 29, 24–26 (2011). 10.1038/nbt.1754 [PubMed: 21221095]
47. Ma H et al. Metabolic rescue in pluripotent cells from patients with mtDNA disease. Nature 524, 234–238 (2015). 10.1038/nature14546 [PubMed: 26176921]
48. Seo JH et al. Syntaphilin Ubiquitination Regulates Mitochondrial Dynamics and Tumor Cell Movements. Cancer Res 78, 4215–4228 (2018). 10.1158/0008-5472.CAN-18-0595 [PubMed: 29898993]
49. Yan Q et al. Proximity labeling identifies a repertoire of site-specific R-loop modulators. Nat Commun 13, 53 (2022). 10.1038/s41467-021-27722-6 [PubMed: 35013239]
50. Cox J & Mann M MaxQuant enables high peptide identification rates, individualized p.p.b.-range mass accuracies and proteome-wide protein quantification. Nat Biotechnol 26, 1367–1372 (2008). 10.1038/nbt.1511 [PubMed: 19029910]
51. Chi H et al. Comprehensive identification of peptides in tandem mass spectra using an efficient open search engine. Nat Biotechnol (2018). 10.1038/nbt.4236

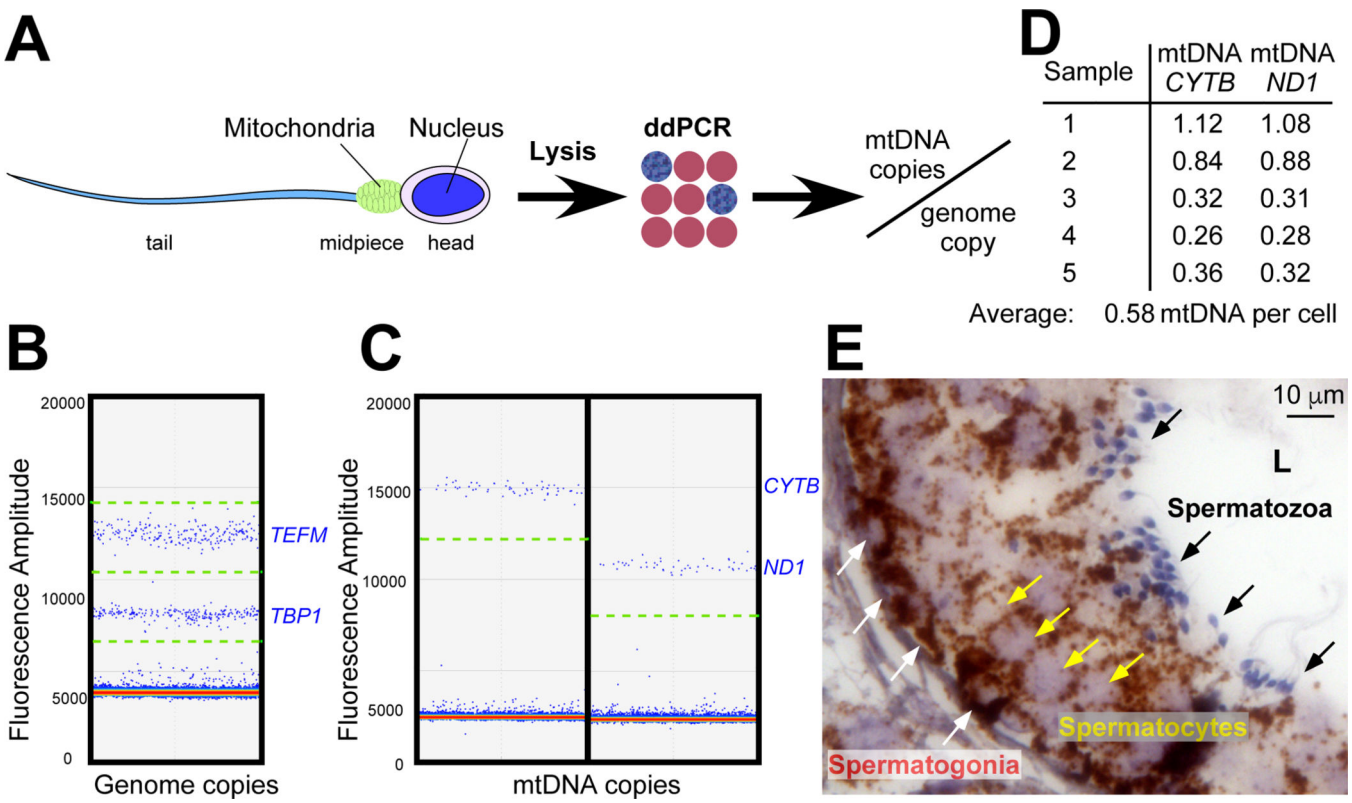

Figure 1. Mitochondria of human spermatozoa contain no mtDNA.

A. Schematics of the mtDNA copy number measurements in sperm cells by ddPCR.

B, C. Representative 1D droplet scatter plots of ddPCR analysis of spermatozoa samples. The multiplex analysis of amplification of two single-copy nuclear genes, TATA-box binding protein 1 and *TEFM* (B), and two mitochondrial genes, cytochrome b and *ND1* (C), in the same spermatozoa sample, is presented. Blue dots above the thresholds (dotted green lines) indicate droplets positive for the target amplicons.

D. Summary data indicating mtDNA copy number per cell.

E. *In situ* RNAScope labeling of mtDNA in developing sperm cells in seminiferous tubules of testicular tissue. MtDNA- brown, white arrows - spermatogonia, yellow – spermatocytes, black – spermatozoa. L – seminiferous tubule lumen.

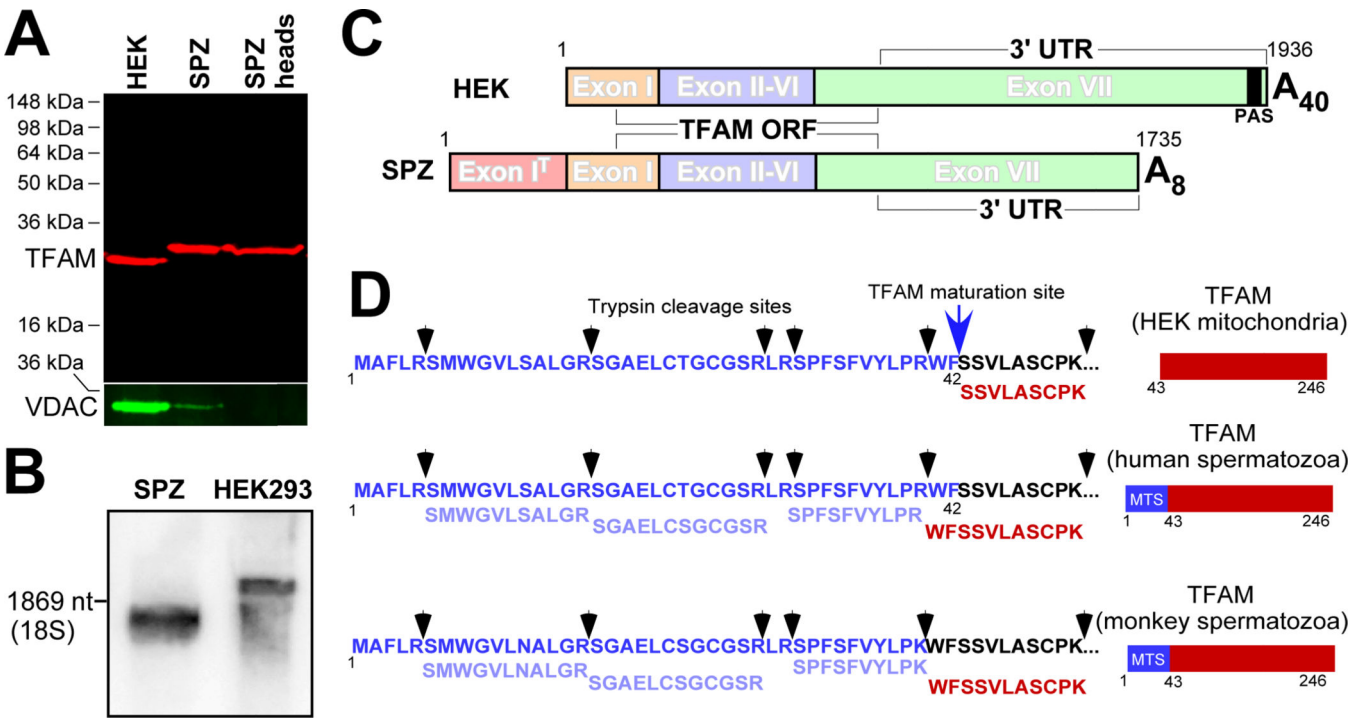

Figure 2. Mature sperm cells contain a specific isoform of TFAM.

A. Western blot of mitochondrial lysate of HEK293 cells (lane 1), spermatozoa (lane 2), and spermatozoa in which the tails/midpieces have been removed (lane 3) are shown. Bottom - Western blot of the same gel stained with the anti-VDAC antibody.

B. Sperm isoform of TFAM is a product of alternative splicing of the TFAM pre-mRNA. Northern blot of mRNA extracted from sperm (SPZ) or HEK293 cells.

C. Schematic illustration of TFAM mRNA structure in somatic and sperm cells.

D. Sperm TFAM isoform contains a mitochondrial pre-sequence, as revealed by LC-MS/MS data. MTS -mitochondrial targeting sequence. Tryptic peptides detected in spermatozoa samples are shown below the N-terminal sequence of TFAM.

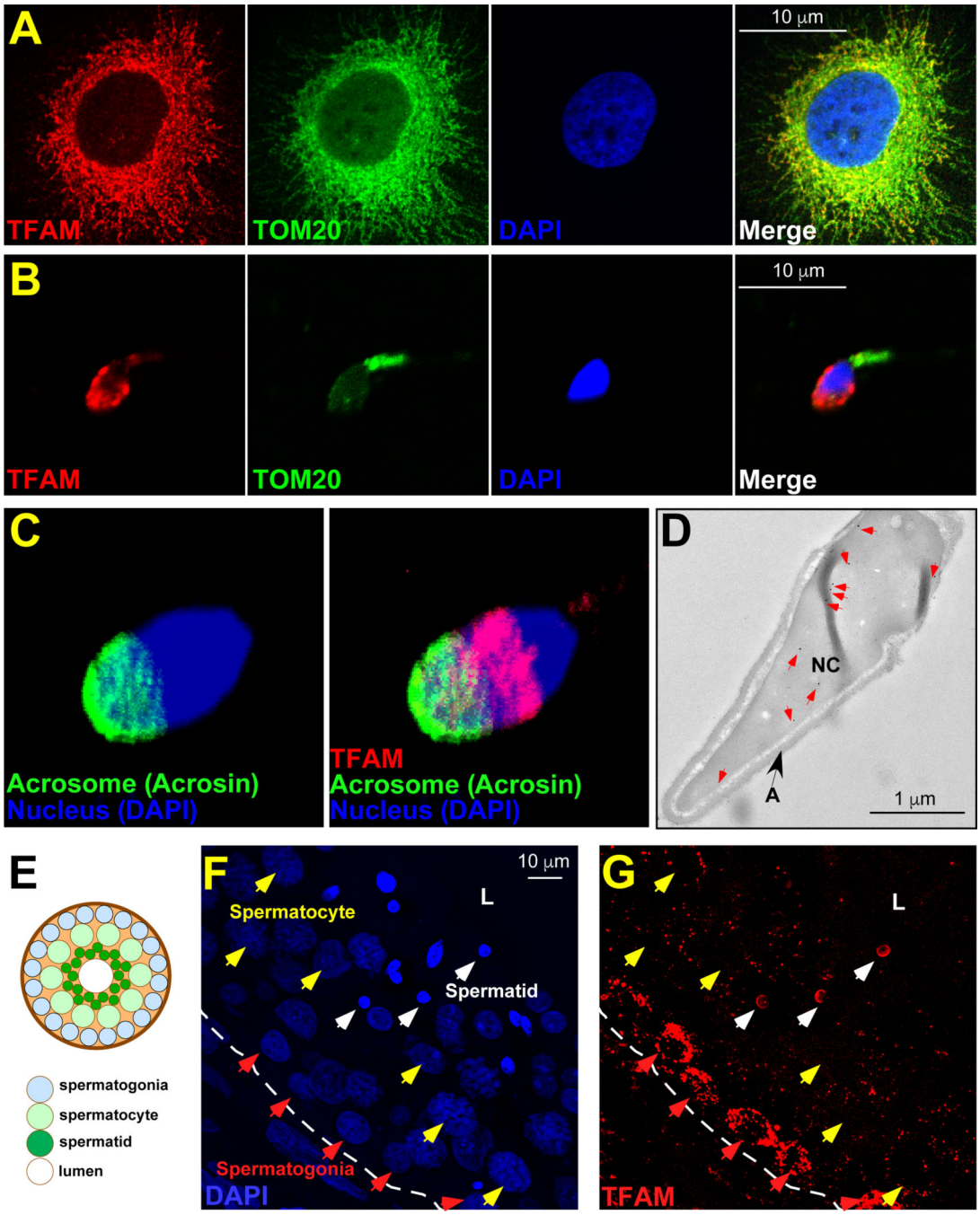

Figure 3. Mature sperm cells contain TFAM in the nucleus but not in the mitochondria.

A, B. Confocal microscopy reveals the localization of the endogenous TFAM (red) in mitochondria of HeLa cells (**A**) and the head of spermatozoa (**B**). Mitochondria staining with an anti-TOM20 antibody (green) and nucleus - DAPI (blue).

C. Deconvolved 3D reconstructed confocal Z-stack image of spermatozoa. Staining with the anti-acrosin antibody (left) or anti-acrosin and anti-TFAM antibody (right).

D. Cryo immunogold electron microscopy to reveal localization of TFAM in spermatozoa. The head region is shown. Red arrows indicate gold particles. A - acrosome, NC- nucleus.

E. Schematic drawing of a transversal cut of a seminiferous tubule.

F, G. Human testicular tissue staining using DAPI (blue, F) and an anti-TFAM antibody (red, G). Red arrows - spermatogonia, yellow – spermatocytes, white – spermatids. The basement membrane is indicated by a dashed line. L – seminiferous tubule lumen.

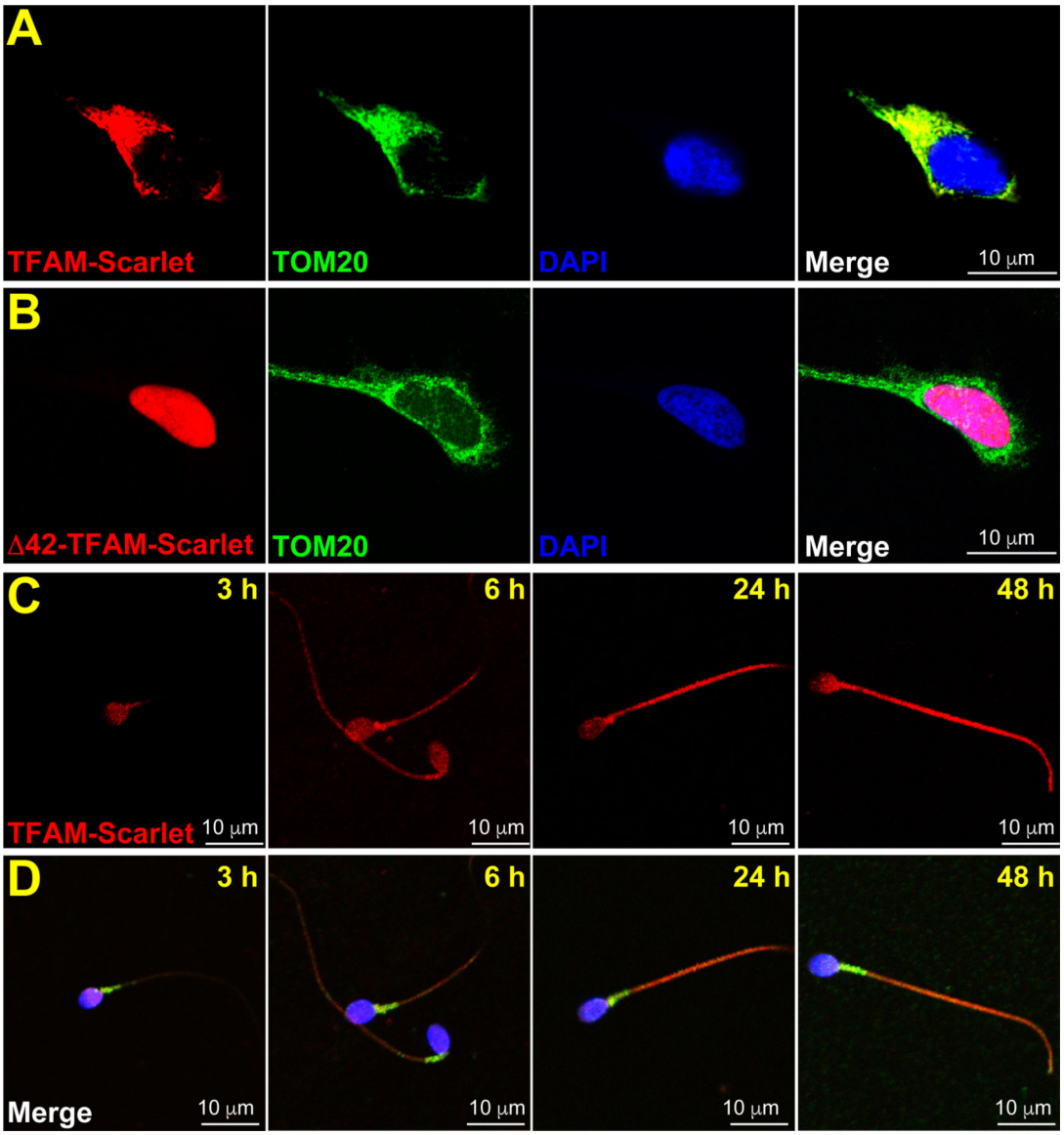

Figure 4. MTS, but not UTR of TFAM mRNA, plays a role in TFAM localization.

A. Confocal microscopy of HeLa cells transduced with the TFAM-mScarlet fusion having the nuclear 3' and 5' UTRs.

B. Confocal microscopy of HeLa cells transduced with TFAM-mScarlet fusion lacking the first 42 amino acids.

C, D. Confocal microscopy of spermatozoa transduced with TFAM-mScalter protein. Mitochondria staining with an anti-TOM20 antibody (green), nucleus - DAPI (blue), TFAM-mScarlet – red.

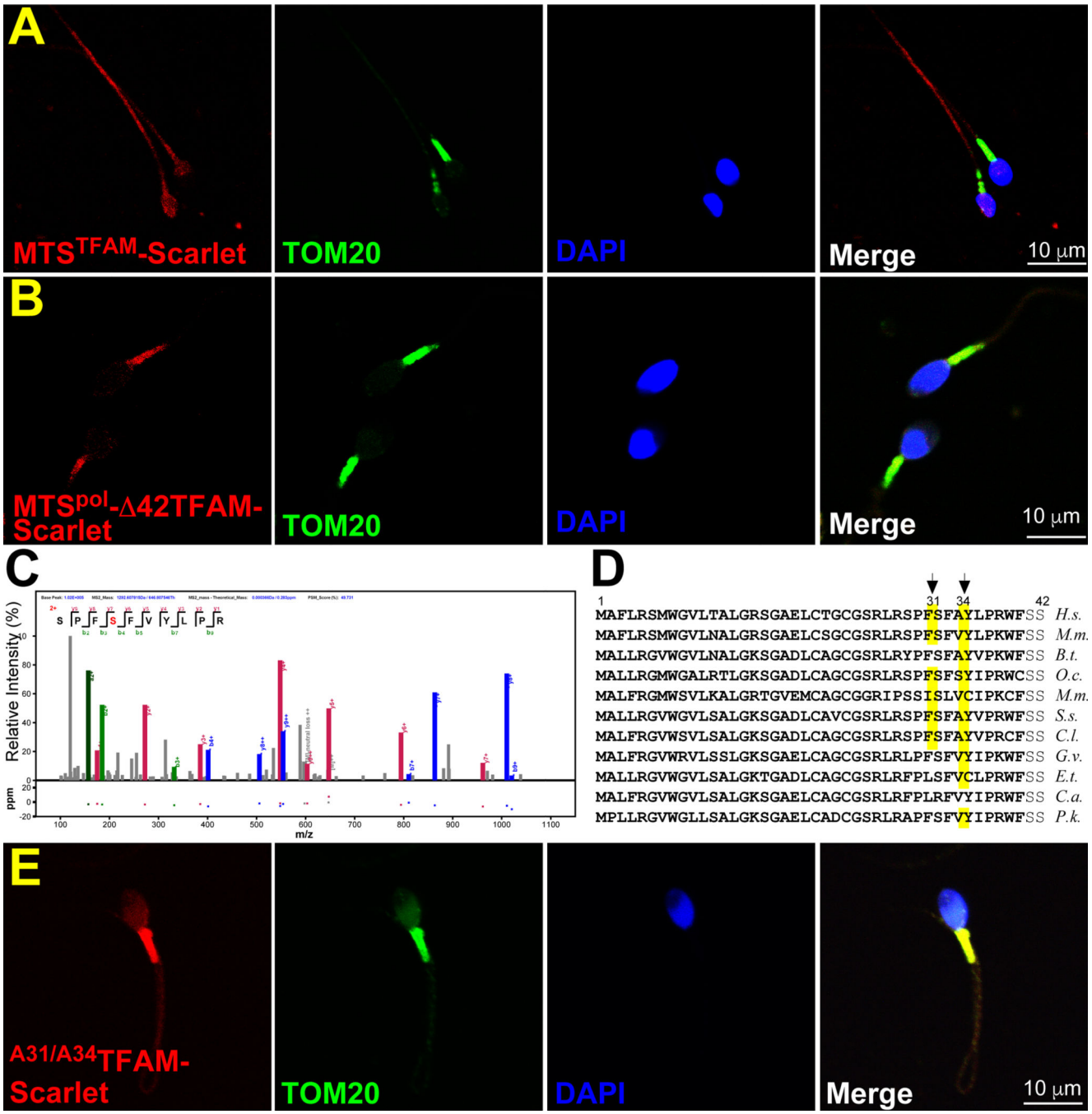

Figure 5. TFAM import to mitochondria is prevented in spermatozoa.

A. Confocal microscopy of spermatozoa transduced with MTS^{TFAM}-mScarlet protein

B. Confocal microscopy of spermatozoa transduced with MTS^{pol}-Δ42TFAM-mScarlet

C. S34 residue in the spermatozoa TFAM pre-sequence is phosphorylated. The MS/MS spectrum confirming the presence of Ser^{34} in TFAM is shown. m/z, mass-to-charge ratio.

D. Conservation of the serine residues implicated in TFAM phosphorylation in mammalian species.

E. Confocal microscopy of spermatozoa transduced with TFAM$^{S31A/S34A}$-mScarlet protein

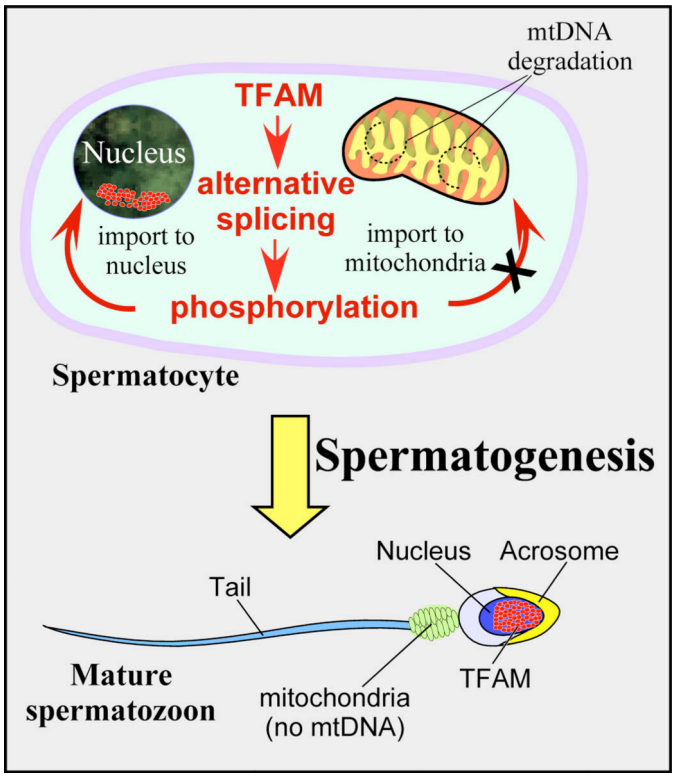

Figure 6. Sperm TFAM re-localization during spermatogenesis.

During spermatogenesis, TFAM is phosphorylated and prevented from being imported to mitochondria, resulting in mtDNA degradation. Instead, TFAM is accumulated in the nucleus of mature spermatozoa.